C5.11 Mathematical Geoscience

Preamble

The course is divided roughly into three sections, on Climate, Rivers, and Glaciers. There will be approximately five lectures on each.

This is primarily a course in mathematical modelling, with application to real world problems. It will use a variety of techniques for developing and solving models based on ordinary and partial differential equations. A certain amount of physics and chemistry will be introduced and translated into the language of differential equations, so an interest in the applications of mathematics to wider branches of science is helpful.

Useful mathematical concepts include Non-dimensionalisation (1st year PDEs, B5.3 Viscous Flow), Linear stability analysis (1st year Dynamics, B5.4 Waves & Compressible Flow), Phase planes (2nd year DEs I), Method of characteristics for first-order hyperbolic equations (2nd year DEs I), Asymptotic methods (2nd year DEs II, C5.5 Perturbation Methods), Lubrication theory (B5.3, C5.7 Topics in Fluids). None of these Part B and C courses are strict pre-requisites.

These notes are based heavily on Andrew Fowler's book 'Mathematical Geoscience' (Springer, 2011), which is the primary reference. The relevant sections are 2.1-2.5; 4.1-4.4; 5.1-5.5; and 10.1-10.4.

Updates 2 December 2017: A number of references to $\sin\theta$ in Sections 3.2 and 3.3 have been corrected to $\tan\theta$ (the bed slope). Marine ice sheets added in Section 3.6. Sections labelled with * in chapter 3 are for interest.

Please send corrections/queries: hewitt@maths.ox.ac.uk

I J Hewitt, December 3, 2017

Contents

1 Climate

1.1 Energy balance models

We begin with a simple climate model to describe the temperature of the Earth's atmosphere.

Most of the mass in the atmosphere is contained within the first 10 km (the troposphere), so we treat it simplistically as a layer of depth $d = 10$ km, average density ρ and temperature T (in fact, the density and temperature both decrease with height in the troposphere, as we discuss more later).

The primary components of the global energy balance are radiative fluxes: we receive shortwave radiation (UV and visible light) from the sun, and emit longwave radiation (infra-red) to space. The balance between these fluxes is the primary factor determining the temperature of the planet. We discuss the theory of radiation in more detail later; for the moment we require only some basic results.

The shortwave radiation received from the sun is $Q \approx 1370$ W m^{-2}. Part of this radiation is absorbed at the Earth's surface, while part is reflected back into space, either from the surface or from clouds in the atmosphere. The fraction reflected is called the albedo, a, and depends on properties of the surface (light surfaces, such as snow, have a high albedo, $a \approx 0.9$; darker surfaces, such as the ocean, have a smaller albedo, $a \approx 0.1$.) The global average albedo is $a \approx 0.3$.

The net shortwave energy flux received from the sun is therefore

$$\pi R^2 Q(1-a), \tag{1.1}$$

where R is the Earth's radius, Q is the solar radiation, and a is the planetary albedo.

A 'black body' with temperature T_e (units K, where 0 C $\approx$ 273 K) emits radiation Q_e (energy per unit time emitted per unit surface area, units W m^{-2}) according to the law,

$$Q_e = \sigma T_e^4, \tag{1.2}$$

where $\sigma \approx 5.67 \times 10^{-8}$ W m^{-2} K^{-4} is the Stefan-Boltzmann constant. (A surface emissivity ε is often included in this law, but we ignore it since it is approximately 1.) The Earth's surface emits radiation according to this law, but some of this longwave radiation is absorbed by the atmosphere and emitted back again. This is the greenhouse effect, which we will discuss further below. It results in the surface temperature T being larger than the *effective emiting temperature* T_e, and we write

$$T_e = \gamma^{1/4} T, \tag{1.3}$$

where $\gamma < 1$ is a greenhouse factor, which depends on the optical thickness of the atmosphere (a function of greenhouse gasses, water vapour, etc.).

The net longwave energy flux radiated from the Earth is therefore

$$4\pi R^2 \sigma \gamma T^4. \tag{1.4}$$

Combining these incoming and outgoing components, the net received radiation over the planetary surface is

$$\pi R^2 Q(1-a) - 4\pi R^2 \sigma \gamma T^4, \tag{1.5}$$

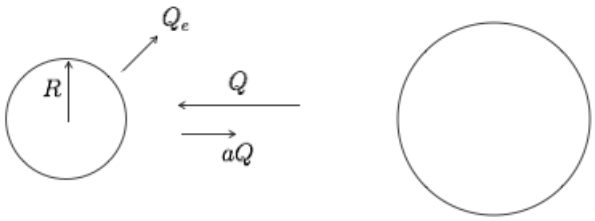

Figure 1.1: The Earth receives shortwave radiative flux Q from the sun and reflects a fraction a. It also emits longwave radiation Q_e.

and this must be equated to the rate of change of the planetary heat content, $4\pi R^2 d\rho c_p T$, where d is the thickness of the atmosphere, ρ is the average density, and c_p is the specific heat capacity of the air. Thus we have

$$c\frac{\mathrm{d}T}{\mathrm{d}t} = \frac{1}{4}Q(1-a) - \sigma\gamma T^4, \tag{1.6}$$

where $c = \rho c_p d$ is the heat capacity of the atmosphere.

This equation has a unique steady state,

$$T = \left(\frac{Q(1-a)}{4\sigma\gamma}\right)^{1/4}. \tag{1.7}$$

The timescale for evolution to the steady state is (balancing terms in the equation),

$$[t] = \frac{d\rho c_p T}{Q(1-a)} \approx 35 \text{ d}, \tag{1.8}$$

using $d \approx 10$ km, $\rho \approx 1$ kg m^{-3}, $c_p \approx 10^3$ J kg^{-1} K^{-1}, $T \approx 288$ K, $Q \approx 1370$ W m^{-2}, and $a \approx 0.3$. This relatively rapid timescale means that the atmosphere responds rapidly to changes in forcing (eg. an increase in CO_2 causing a decrease in γ).

If we take $\gamma = 1$, the equilibrium temperature for the Earth is predicted to be $T \approx 255$ K, compared to the actual average temperature of around 288 K. We see that the greenhouse effect is important in keeping the Earth warm enough for us to live on; the value of γ inferred from (1.3) is $\gamma \approx 0.61$.

The same simple model can be used to estimate the equilibrium temperature of other planets. The solar radiation falls off with the inverse square of distance from the sun, so if planetary albedos were the same, the temperatures would fall off as the 1/8th power of distance from the sun. However the albedo depends on surface and atmosphere properties and varies significantly between planets, so the relationship is not so straightforward. In addition, the greenhouse factor γ is different for each planet.

Taking $\gamma = 1$ for Venus, with $Q \approx 2640$ W m^{-2} and $a \approx 0.77$, would give $T \approx 230$ K, whereas the actual surface temperature averages around 740 K. We infer that the greenhouse factor for Venus is $\gamma \approx 0.01$, so the greenhouse effect is much stronger than on Earth.

1.2 Radiation and the greenhouse factor

Here we describe some basic theory of radiative energy transfer, with the goal to provide a description of the greenhouse effect.

Figure 1.2: Radiative intensity is a function of position $\mathbf{x}$ and direction $\hat{\mathbf{s}} = (\sin\theta\cos\phi, \sin\theta\sin\phi, \cos\theta)$. An element of solid angle has projected area on the unit sphere $\mathrm{d}\omega = \sin\theta \mathrm{d}\theta\mathrm{d}\phi$.

1.2.1 Radiative energy transfer

Radiation is the transfer of energy by electromagnetic waves. At each point in space the wave field can be broken down into waves of different frequencies travelling in different directions. We define the intensity

$$I_\nu(\mathbf{x}, \hat{\mathbf{s}}), \tag{1.9}$$

as the energy flux per unit surface area of waves with frequency ν travelling in direction $\hat{\mathbf{s}}$, at position $\mathbf{x}$. Frequency is related to wavelength by $\lambda = c/\nu$, where c is the speed of light. The total radiative energy flux may be written as

$$\mathbf{q}(\mathbf{x}) = \int_\circ \int_0^\infty I_\nu(\mathbf{x}, \hat{\mathbf{s}})\hat{\mathbf{s}}\ \mathrm{d}\nu\ \mathrm{d}\omega, \tag{1.10}$$

where the first integral is taken over all frequencies ν and the second is taken over all directions, where $\mathrm{d}\omega = \mathrm{d}\omega(\hat{\mathbf{s}})$ is the element of solid angle associated with direction $\hat{\mathbf{s}}$. Solid angle is the three-dimensional generalisation of a normal angle, and can be thought of as the projected area of a beam onto a unit sphere. In terms of the two polar angles, $\hat{\mathbf{s}} = (\sin\theta\cos\phi, \sin\theta\sin\phi, \cos\theta)$, and $\mathrm{d}\omega = \sin\theta\ \mathrm{d}\theta\ \mathrm{d}\phi$.

The radiative transfer equation describes the rate of change of intensity I_ν in direction $\hat{\mathbf{s}}$,

$$\frac{\partial I_\nu}{\partial s} = -\rho\kappa_\nu I_\nu + \rho\kappa_\nu B_\nu. \tag{1.11}$$

Here, $\partial/\partial s = \hat{\mathbf{s}} \cdot \nabla_{\mathbf{X}}$. The first term describes absorption by the atmosphere and the second term describes re-emission, where ρ is the density and κ_ν are absorption coefficients. Re-emssion is assumed to be independent of direction (i.e. independent of $\hat{\mathbf{s}}$) and is described by the Planck function

$$B_\nu = \frac{2h\nu^3}{c^2(e^{h\nu/kT} - 1)}, \tag{1.12}$$

which describes the emission of radiation for given local temperature T. Here $h \approx 6.6 \times 10^{-34}$ J s is Planck's constant, $c \approx 3.0 \times 10^8$ m s^{-1} is the speed of light, and $k \approx 1.38 \times 10^{-23}$ J K^{-1} is Boltzmann's constant.

In reality the atmosphere absorbs radiation of different frequencies at different rates (depending on its composition), so that κ_ν are strongly dependent on frequency, and the radiative transfer equation (1.11) must be solved separately for each frequency. To make analytical progress,

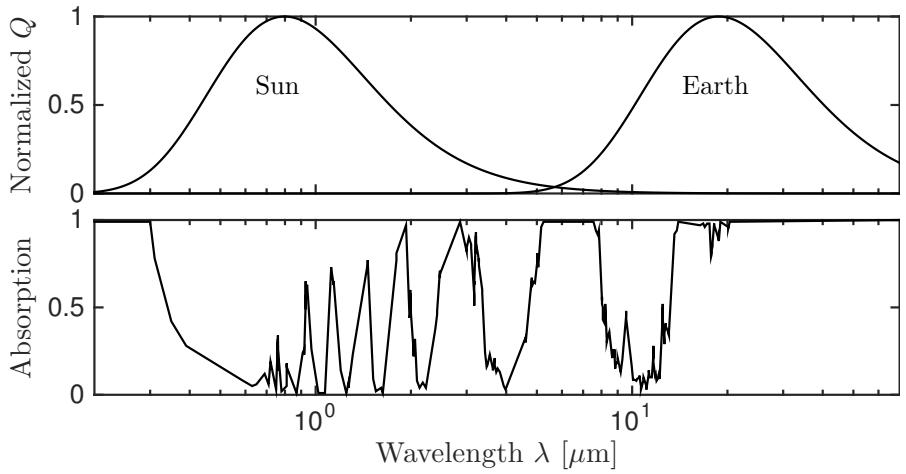

Figure 1.3: Black body emission from the Sun (~ 6000 K) and the Earth (~ 255 K), together with atmospheric absorption for different wavelengths.

however, we make the approximation that the atmosphere is 'grey', meaning that $\kappa_\nu = \kappa$ is independent of frequency.

We can then define the total radiation intensity and emission intensity as

$$I(\mathbf{x}, \mathbf{s}) = \int_0^\infty I_\nu \, \mathrm{d}\nu, \qquad B(\mathbf{x}) = \int_0^\infty B_\nu \, \mathrm{d}\nu, \tag{1.13}$$

and integrate the radiative transfer equation assuming $\kappa_\nu = \kappa$ to give

$$\frac{\partial I}{\partial s} = -\rho\kappa(I - B). \tag{1.14}$$

In fact, a truly grey atmosphere is not a good approximation. Some frequencies are much more strongly absorbed, but there are 'windows' in the absorption spectrum that allow more effective transmission of short wave radiation ($\lambda \approx 0.3 - 1$ μm, including visible light), and long wave radiation ($\lambda \approx 8 - 14$ μm). We are mostly interested in the latter window (the greenhouse effect depends on how much of the longwave radiation emitted from the Earth's surface is absorbed and emitted back again), and can effectively consider just the frequency/wavelength range corresponding to this window. By assuming the absorption coefficient is independent of frequency *within* that window, we may still make use of the grey approximation.

If we also make the assumption of *local radiative equilibrium*, which assumes that radiation is the only heat transfer mechanism, then B must be equal to the average of the radiation over all directions at each point,

$$B(\mathbf{x}) = \frac{1}{4\pi} \int_0^{2\pi} \int_0^\pi I(\mathbf{x}, \hat{\mathbf{s}}) \sin\theta \, \mathrm{d}\theta \, \mathrm{d}\phi. \tag{1.15}$$

This statement is due to energy conservation, because the energy absorbed and emitted by an infinitesimal parcel of the medium must be equal in the absence of other methods of energy transfer.

Note that (1.12) can be integrated (exercise) to give,

$$B = \frac{\sigma T^4}{\pi}, \tag{1.16}$$

where $\sigma = 2\pi^5 k^4/15h^3c^2$ is the Stefan-Boltzmann constant, so that B is also related to the local temperature at each point.

1.2.2 Two-stream approximation

We consider a one-dimensional atmosphere so $I = I(z, \theta)$, where θ is the angle of $\hat{\mathbf{s}}$ to the vertical. Then $\partial/\partial s = \cos\theta \partial/\partial z$, so the radiative transfer equation becomes

$$\cos\theta \frac{\partial I}{\partial z} = -\rho\kappa(I - B). \tag{1.17}$$

Since ρ may depend on z, it is helpful to define a new vertical coordinate, the optical depth τ, by

$$\tau = \int_z^\infty \rho\kappa \, \mathrm{d}z. \tag{1.18}$$

If we also write $\mu = \cos\theta$, then $I = I(\tau, \mu)$ satisfies

$$\mu \frac{\partial I}{\partial \tau} = I - B, \tag{1.19}$$

where the radiative equilibrium assumption is

$$B = \frac{1}{4\pi} \int_0^{2\pi} \int_0^{\pi} I \sin\theta \, \mathrm{d}\theta \, \mathrm{d}\phi = \frac{1}{2} \int_{-1}^{1} I(\tau, \mu) \, \mathrm{d}\mu. \tag{1.20}$$

We next make an approximation (the Schuster-Schwarzschild approximation) to reduce all the different directions of radiation to just two averages, over upwards and downwards directions,

$$I_+ = \frac{1}{2\pi} \int_0^{2\pi} \int_0^{\pi/2} I \sin\theta \, \mathrm{d}\theta \, \mathrm{d}\phi = \int_0^1 I \, \mathrm{d}\mu, \tag{1.21}$$

$$I_- = \frac{1}{2\pi} \int_0^{2\pi} \int_{\pi/2}^{\pi} I \sin\theta \, \mathrm{d}\theta \, \mathrm{d}\phi = \int_{-1}^0 I \, \mathrm{d}\mu. \tag{1.22}$$

The net upwards and downwards radiative fluxes (*i.e.* the vertical components $I(z, \theta)\cos\theta$) are given by

$$F_+ = \int_0^{2\pi} \int_0^{\pi/2} I \cos\theta \sin\theta \, \mathrm{d}\theta \, \mathrm{d}\phi = 2\pi \int_0^1 I\mu \, \mathrm{d}\mu \approx \pi I_+, \tag{1.23}$$

$$F_- = -\int_0^{2\pi} \int_{\pi/2}^{\pi} I \cos\theta \sin\theta \, \mathrm{d}\theta \, \mathrm{d}\phi = -2\pi \int_{-1}^0 I\mu \, \mathrm{d}\mu \approx \pi I_-, \tag{1.24}$$

where the final approximations are based on the fact that $\int_0^1 \mu \, \mathrm{d}\mu = \frac{1}{2}$.

Using this same approximation, we can integrate (1.19) with respect to μ (from -1 to 0 and from 0 to 1) to give

$$\frac{1}{2}\frac{\mathrm{d}I_+}{\mathrm{d}\tau} = I_+ - B, \tag{1.25}$$

$$-\frac{1}{2}\frac{\mathrm{d}I_-}{\mathrm{d}\tau} = I_- - B. \tag{1.26}$$

With the local radiative equilibrium assumption, $B = \frac{1}{2}(I_+ + I_-)$, these become

$$\frac{\mathrm{d}I_+}{\mathrm{d}\tau} = \frac{\mathrm{d}I_-}{\mathrm{d}\tau} = I_+ - I_-. \tag{1.27}$$

Boundary conditions are $I_- = 0$ at $\tau = 0$, which expresses the fact that there is no incoming radiation at the top of the atmosphere, and $\pi I_+ = \sigma T_s^4$, which expresses the flux from the surface according to the Stefan-Boltzmann law, where T_s is the surface temperature.

Subtracting (1.26) from (1.25) we see that the net upwards flux $F = F_+ - F_- = \pi(I_+ - I_-)$ is constant (independent of τ), and each of the equations can therefore be integrated to give

$$F_- = \pi I_- = F\tau, \qquad F_+ = \pi I_+ = F(1+\tau). \tag{1.28}$$

The surface boundary condition therefore gives

$$F = \frac{\sigma T_s^4}{1+\tau_s}, \tag{1.29}$$

where $\tau_s = \int_0^\infty \rho\kappa \, \mathrm{d}z$ is the optical thickness of the atmosphere.

Note that the net upwards flux F defines the effective emitting temperature T_e according to

$$F = \sigma T_e^4, \tag{1.30}$$

and therefore

$$T_s = (1+\tau_s)^{1/4} T_e. \tag{1.31}$$

This explains why the surface temperature is warmer than the effective emitting temperature, and we may read off how the greenhouse factor γ, defined earlier, is related to the optical thickness of the atmosphere,

$$\gamma = \frac{1}{1+\tau_s}. \tag{1.32}$$

Moreover, $B = F(\frac{1}{2} + \tau)/\pi$, so the atmospheric temperature T from (1.16) is related to T_e by

$$T = \left(\frac{\frac{1}{2}+\tau}{1+\tau_s}\right)^{1/4} T_e, \tag{1.33}$$

which suggests that the temperature decreases with height.

In reality, this expression does not well describe the temperature variation with height, because the assumption of local radiative equilibrium is not valid. Convection and moisture transport are also important mechanisms of heat transport within the atmosphere.

1.3 The runaway greenhouse effect

The optical thickness of the atmosphere depends on its composition. Water vapour, carbon dioxide, methane, and other gasses contribute to increasing the absorption coefficient κ, which in turn causes an increase in the optical thickness τ_s and a decrease in the greenhouse factor γ.

An interesting question is what determines this value, and why there appears to be a large difference in the greenhouse factor between Earth and Venus. We have seen that an increase in the greenhouse effect results in larger surface temperature, which we would expect to enhance

evaporation and therefore increase the quantity of water vapour in the atmosphere. This provides a positive feedback, resulting in continued increase in temperature.

During the formation of the Earth's early atmosphere, the positive feedback was most likely limited by the formation of clouds. Clouds (liquid water droplets) form when the air becomes saturated with water vapour, resulting in condensation and eventually rain, which removes water from the atmosphere. A possible explanation for the high temperatures on Venus is that this limiting process did not apply, leading to a continued increase in temperature and vapour content (eventually, UV radiation causes dissociation of H_2O into H_2 and O_2, and the hydrogen escapes into space).

The amount of water vapour in the atmosphere can be described in terms of the partial vapour pressure p_v, or the water vapour density ρ_v (mass of water vapour molecules per unit volume). These are related by the ideal gas law

$$p_v = \frac{\rho_v R T}{M_v}, \tag{1.34}$$

where R is the gas constant, T the temperature and M_v the molecular weight. However, for a given temperature there is a maximum possible vapour pressure, the saturation vapour pressure $p_{sv}(T)$, which varies with temperature according to the Clausius-Clapeyron relation

$$\frac{\mathrm{d}p_{sv}}{\mathrm{d}T} = \frac{\rho_v L}{T}, \tag{1.35}$$

were L is the latent heat. If p_v reaches p_{sv} it cannot increase further without the atmosphere becoming supersaturated. Instead, the partial pressure becomes constrained to p_{sv}, and any further increase in water content results in condensation to produce clouds, which subsequently produce rain and remove the excess water from the atmosphere. The slope of this saturation curve may be combined with the ideal gas law (with $p_v = p_{sv}$) to obtain

$$\ln \frac{p_{sv}}{p_{sv0}} = \frac{M_v L}{R T_0}\left(1 - \frac{T_0}{T}\right), \tag{1.36}$$

were p_{sv0} is the reference value at temperature T_0.

As an illustration, suppose we approximate the dependence of the greenhouse factor on water vapour by $\gamma \approx 1/\tau_s \approx K/\rho_v$, where K is a constant. The equilibrium temperature from (1.7) is then

$$T = \left(\frac{Q(1-a)}{4\sigma K}\rho_v\right)^{1/4}, \tag{1.37}$$

or, using the ideal gas law,

$$T = \left(\frac{Q(1-a)M_v}{4\sigma K R}p_v\right)^{1/5}. \tag{1.38}$$

During the early stages of formation of the planetary atmosphere (there was initially no atmosphere or indeed ocean), we presume that water vapour and other dissolved gases were released by volcanism from the planet's interior. This resulted in a slow increase in the partial vapour pressure, and hence an increase in temperature described by (1.38). There is a corresponding increase in the saturation vapour pressure according to (1.36). Depending on the relative rates of increase of p_v and p_{sv}, there are two options: either the partial pressure reaches the saturation pressure and clouds form, preventing further increase in T; or the

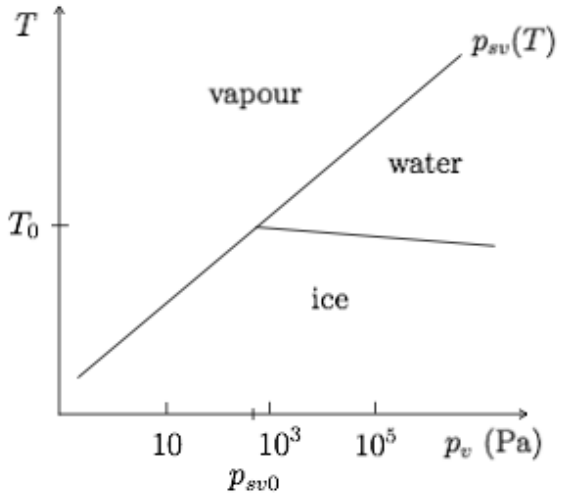

Figure 1.4: Phase diagram for water, with triple point at temperature $T_0 \approx 273$ K and partial vapour pressure $p_{sv0} \approx 612$ Pa. The phase boundaries are given by the Clausius-Clapeyron relations.

partial pressure remains below the saturation value (which itself increases with temperature), in which case the temperature continues to increase.

Which of these possibilities occurs depends on whether the curves described by (1.36) and (1.38) intersect. If we approximate $1 - T_0/T \approx (T - T_0)/T_0$, based on $T \approx T_0$, write $T = T_0\theta$, $p_v = p_{sv0}e^{5\xi_v}$, and $p_{sv} = p_{sv0}e^{5\xi_{sv}}$, these curves can be written as

$$\theta = 1 + \alpha\xi_{sv}, \qquad \theta = \beta e^{\xi_v}, \tag{1.39}$$

where

$$\alpha = \frac{5RT_0}{M_v L}, \qquad \beta = \left(\frac{Q(1-a)M_v p_{sv0}}{4\sigma K R T_0^5}\right)^{1/5}. \tag{1.40}$$

These do not intersect if

$$\beta > \beta_c = \alpha \exp\left(\frac{1-\alpha}{\alpha}\right), \tag{1.41}$$

(the limiting case occurs when the curves meet tangentially). Non-intersection, leading to the runaway greenhouse effect, therefore occurs if the solar radiation Q is sufficiently large. This indicates the distinction between Earth and Venus, for which the value of Q is approximately twice as large (the critical flux depends on the value of the constant K, but the situation in reality is more complicated because the greenhouse factor does not only depend on water vapour).

1.4 Vertical structure of the atmosphere

Until now we have largely ignored the vertical density and temperature variations within the atmosphere (although we considered the temperature profile in a purely radiative atmosphere).

The pressure decreases with height due to the decreasing weight of the overlying air column. Vertical force balance gives

$$\frac{\mathrm{d}p}{\mathrm{d}z} = -\rho g, \tag{1.42}$$

and the ideal gas law relates pressure and density according to

$$p = \frac{\rho R T}{M_a}, \tag{1.43}$$

where R is the gas constant, T is the temperature and M_a is the molecular weight. Since the absolute temperature does not vary hugely over most of the atmosphere, a reasonable approximation of the density profile may be obtained by taking it as constant. Then the force balance becomes

$$-\frac{1}{\rho}\frac{\mathrm{d}\rho}{\mathrm{d}z} \approx \frac{M_a g}{RT}, \tag{1.44}$$

so ρ decreases approximately exponentially with height, over a length scale called the *scale height*,

$$H = \frac{RT}{M_a g} \approx 8 \text{ km}, \tag{1.45}$$

using values $T = 273$ K, $R = 8.3$ J K^{-1} mol^{-1}, $M_a = 28.8 \times 10^{-3}$ kg mol^{-1}, and $g = 9.8$ m s^{-2}. Similarly, the pressure also decreases approximately exponentially with height.

To go further and understand the temperature structure, we must also consider energy balance. The energy equation in a dry atmosphere (neglecting phase changes) is

$$\rho c_p \frac{\mathrm{D}T}{\mathrm{D}t} - \beta T \frac{\mathrm{D}p}{\mathrm{D}t} = \nabla \cdot (k \nabla T) - \nabla \cdot \mathbf{q}, \tag{1.46}$$

where the material derivatives, representing the rate of change following fluid parcels, are given in terms of velocity $\mathbf{u}$ by

$$\frac{\mathrm{D}f}{\mathrm{D}t} = \frac{\partial f}{\partial t} + \mathbf{u} \cdot \nabla f. \tag{1.47}$$

The terms on the left represent the advection of sensible heat and the work of thermal compression ($\beta = -\rho^{-1}\partial\rho/\partial T$ is the thermal expansion coefficient, equal to $1/T$ for an idea gas), and the terms on the right represent heat transfer by conduction and radiation. The latter was considered earlier, and is fundamentally important in determining energy transfer to and from the atmosphere. However, if we consider only the lower 10 km (the troposphere), the dominant energy transfer process *within* this region is convection, described by the terms on the left.

Convection occurs as a result of thermal expansion (warm air is lighter) and an unstable stratification. The temperature is usually higher nearer the ground and convective overturning is therefore widespread. (Temperature inversions, when colder air lies stably beneath warmer air, do sometimes occur, often at night under clear sky when the long wave radiative loss from he Earth is larger; the colder air can hold less water vapour and often results in low-lying clouds in valleys).

A one-dimensional steady state balance of the advective terms in (1.46), together with the ideal gas law, gives

$$\rho c_p \frac{\mathrm{d}T}{\mathrm{d}z} - \frac{\mathrm{d}p}{\mathrm{d}z} = 0, \tag{1.48}$$

and combing with the force balance (1.42) gives

$$\frac{\mathrm{d}T}{\mathrm{d}z} = -\frac{g}{c_p} \approx -10 \text{ K km}^{-1}. \tag{1.49}$$

This value is sometimes refered to as the dry adiabatic lapse rate. However, the average lapse rate of the Earth's atmosphere is closer to 6 K km^{-1}, due to the presence of water vapour and the heat associated with its condensation. The amount of water vapour can be expressed in terms of the mixing ratio

$$m = \frac{\rho_v}{\rho}, \tag{1.50}$$

where ρ_v is the water vapour density and ρ the total air density (typically $m \approx 0.02$, so the impact of water vapour on ρ is small). Alternatively we may express the amount of water vapour using the ideal gas law in terms of the partial vapour pressure,

$$p_v = \frac{\rho_v R T}{M_v}. \tag{1.51}$$

If the partial pressure reaches the saturation vapour pressure $p_{sv}(T)$, given by the Clausius-Clapeyron equation

$$\frac{\mathrm{d}p_{sv}}{\mathrm{d}T} = \frac{\rho_v L}{T}, \tag{1.52}$$

then condensation occurs so as to maintain $p_v = p_{sv}$. This condensation produces water droplets (clouds) which then grow and fall as rain. For unsaturated air, the ratio p_v/p_{sv} is the relative humidity, which measures how close the air is to saturation. Condensation acts as a heat source, so the energy equation (1.46) for a moist (saturated) atmosphere is modified to

$$\rho c_p \frac{\mathrm{D}T}{\mathrm{D}t} - \frac{\mathrm{D}p}{\mathrm{D}t} + \rho L \frac{\mathrm{D}m}{\mathrm{D}t} = 0, \tag{1.53}$$

(the conduction and radiation terms on the right are ignored). For a one-dimensional steady state dominated by convection, we have

$$\rho c_p \frac{\mathrm{d}T}{\mathrm{d}z} - \frac{\mathrm{d}p}{\mathrm{d}z} + \rho L \frac{\mathrm{d}m}{\mathrm{d}z} = 0, \tag{1.54}$$

and using the ideal gas laws combined with the saturation condition $p_v = p_{sv}$, we can find (exercise),

$$\frac{\mathrm{d}T}{\mathrm{d}z} = -\frac{g}{c_p}\left[\frac{1 + \frac{\rho_v L}{p}}{1 + \frac{\rho_v L}{p}\frac{M_v}{M_a}\frac{L}{c_p T}}\right] \approx 5.4 \text{ K km}^{-1}. \tag{1.55}$$

Here we have used values $M_v = 18 \times 10^{-3}$ kg mol^{-1}, $M_a = 29 \times 10^{-3}$ kg mol^{-1}, $L = 2.5 \times 10^6$ J kg^{-1}, $g = 9.8$ m s^{-2}, and $c_p = 10^3$ J kg^{-1} K^{-1}, and take $\rho_v \approx 0.01$ kg m^{-3}, $p \approx 10^6$ Pa, $T \approx 300$ K (ρ_v, p and T all vary with altitude, but the *variation* is relatively small, so the lapse rate is approximately constant).

The above discussion applies to the *troposphere*, the lower approximately 10 km of the atmosphere. The convection due to the unstable stratification, and on a larger planetary scale due to differential heating between equator and poles, gives rise to large scale motions of the atmosphere that we think of as the weather. The top of the troposphere is called the *tropopause*, and is distinguished by a temperature minimum of around 210 K, which occurs at around 10 km (it is higher nearer the equator). Commercial aeroplanes usually fly close to this altitude, where the air density is lower and therefore provides less drag.

Above the tropopause lies the *stratosphere*, in which the temperature increases again with height to reach another maximum of around 270 K at the *stratopause*, around 50 km up. The stratosphere is therefore stably stratified and lacks the convective motions of the troposphere.

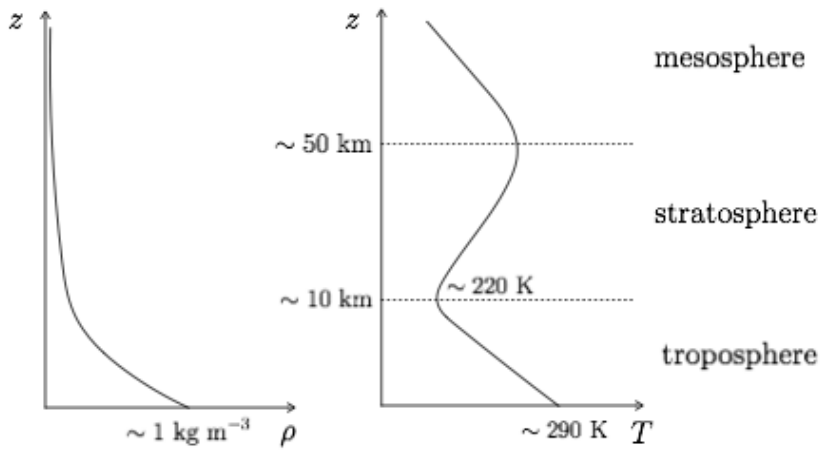

Figure 1.5: Density and temperature structure of the atmosphere as a function of height.

The temperature increase is due to the absorption of short wave (UV) solar radiation by ozone, which provides a significant internal heat source (the second term on the right of (1.46)).

Above the stratosphere is the *mesosphere* in which temperature again decreases with height, and then above about 80 km is the *thermosphere*, in which temperature increases again.

1.5 Ice-albedo feedback

The planetary albedo depends on the relative proportion of ocean, snow, forest, deserts, etc over the Earth's surface. The amount of sea ice and land ice, which has a high albedo, can have a very pronounced effect on the climate, and provide a positive feedback that helps to explain the occurrence of ice ages.

Ice ages have occurred periodically for the last 2 million years, as evidenced by Antarctic ice cores and ocean-floor sediment cores. During the ice ages, ice sheets covered much of northern Europe (the Fenno-scandian ice sheet) and North America (the Laurentide ice sheet). The ice locked up in these ice sheets caused the sea level to be around 130 metres lower than it is today (for comparison, the current-day ice sheets of Greenland and Antarctica contain ice equivalent to around 65 metres of average sea level). The last glacial period ended quite abruptly around 10 thousand years ago, and we are currently in an *interglacial* period.

The timing of the ice ages is believed to relate to changes in solar forcing ($\approx 5\%$) that are due to slight variations in the Earth's orbit. The theory that these orbital variations are responsible for climate cycles is due to Milanković. There are three primary components to the orbital variations: the precision of the Earth's axis (which occur on a roughly 21 ky cycle), changes in the tilt of the axis (41 ky), and changes in the eccentricity of the elliptical orbit (100 ky).

On their own, the variations are not thought to be sufficient to explain the large temperature change between and glacial and interglacial periods (≈ 10 K), or their timing. However, the ice-albedo feedback can help to accentuate the change.

We can write the atmospheric energy balance (1.6) as

$$c\frac{\mathrm{d}T}{\mathrm{d}t} = R_i - R_o, \qquad R_i = \frac{1}{4}Q(1-a), \qquad R_o = \sigma\gamma T^4, \tag{1.56}$$

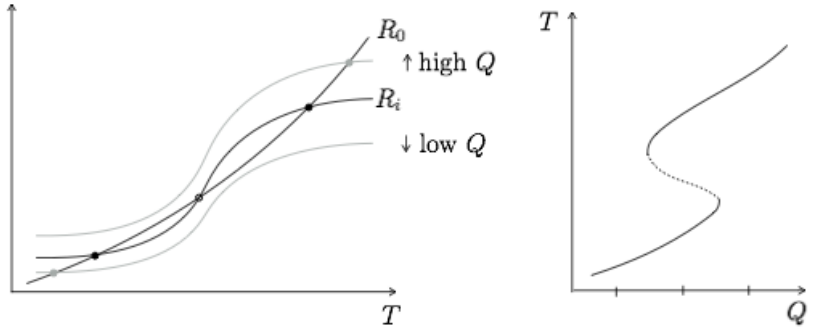

Figure 1.6: (a) Incoming and outgoing radiative fluxes as a function of temperature, for different values of solar flux Q. (b) Steady state temperature (from the intersections of R_i and R_o) as a function of solar flux.

but now take the planetary albedo a to be a monotonically decreasing function of temperature, since we associate lower temperatures with greater ice cover. For example,

$$a(T) = a_+ - (a_+ - a_-)\frac{1}{2}\left[1 + \tanh\left(\frac{T - T_m}{\Delta T}\right)\right]. \tag{1.57}$$

We could also take γ to depend on temperature (due to varying amounts of atmospheric water vapour), but for simplicity we here keep it as constant.

Plotting the incoming and outgoing fluxes, $R_i(T)$ and $R_o(T)$, we see that there is the potential for multiple steady states, providing the dependence of a on T is strong enough, and provided Q is within a certain range.

Moreover, plotting $\mathrm{d}T/\mathrm{d}t$ as a function of T, we see that if there are multiple steady states, the lower and upper ones are stable and the middle one is unstable (as is typical for this type of system).

The stability can also be confirmed using a linear stability analysis, writing $T = T_0 + \theta$, where T_0 is the steady state and $\theta \ll T_0$, so that

$$\frac{\mathrm{d}\theta}{\mathrm{d}t} \approx \big(R_i'(T_0) - R_o'(T_0)\big)\theta, \tag{1.58}$$

indicating that the steady state is stable (the perturbation θ decays) provided $R_o'(T_0) > R_i'(T_0)$.

Varying Q can cause multiple steady states to come and go. If Q is too small, only a low temperature solution exists (an ice age), and if Q is too large, only a high temperature solution exists (an interglacial). Orbital variations of Q between these values can cause jumps from the warm to the cold branches, which correspond to the inception and termination of an ice age.

The simple model in (1.56) does not correctly describe the timescale of climate change associated with ice ages, because we assumed a steady state relationship between the albedo and temperature, whereas in reality the timescale for adjustment of the albedo (due to the growth of ice sheets) is quite long. In fact this is by far the rate-limiting process, and the energy balance (1.56) can effectively be taken to be in a steady state. Such behaviour, when the time derivative is negligible on the longer timescales of interest, is referred to as *quasi-steady*, and the approximation to neglect the time derivative completely is referred to as a quasi-steady approximation.

To account for the longer timescale, a simple phenomenological model is

$$c\frac{\mathrm{d}T}{\mathrm{d}t} = \frac{1}{4}Q(1-a) - \sigma\gamma T^4, \tag{1.59}$$

$$t_i\frac{\mathrm{d}a}{\mathrm{d}t} = a_0(T) - a, \tag{1.60}$$

where $a_0(T)$ is the equilibrium albedo for a given temperature, given by (1.57) for instance, and where $t_i \approx 10$ ky is the timescale associated with changes in ice cover.

If this equation is non-dimensionalised, by writing

$$Q \sim [Q]\hat{Q}, \qquad T \sim [T]\hat{T}, \qquad t \sim [t]\hat{t}, \tag{1.61}$$

and choosing $[t] = t_i$ and $[T] = ([Q]/4\sigma\gamma)^{1/4}$, we obtain

$$\varepsilon\frac{\mathrm{d}\hat{T}}{\mathrm{d}\hat{t}} = \hat{Q}(1-a) - \hat{T}^4, \qquad \frac{\mathrm{d}a}{\mathrm{d}t} = a_*(\hat{T}) - a, \tag{1.62}$$

where $\varepsilon = 4c[T]/t_i[Q] \ll 1$ is the ratio of timescales for temperature and albedo adjustment (and $a_*(\hat{T}) = a_0(T)$ is the equilibrium albedo expressed as a function of dimensionless temperature).

The quasi-steady approximation is to take $\varepsilon \to 0$, so that $\hat{T} = \hat{T}(a) = [Q(1-a)]^{1/4}$, and then

$$\frac{\mathrm{d}a}{\mathrm{d}t} = a_*(\hat{T}(a)) - a. \tag{1.63}$$

The steady states and stability of this differential equation can be analysed as for (1.56), with the same conclusions.

1.6 Carbon

In this section we extend the simple climate models above to include atmospheric and ocean carbon dioxide. We are partly interested in understanding the changes that are likely to occur due to human carbon emissions, and partly interested in whether feedbacks exist that can help to explain aspects of the ice-age cycles.

1.6.1 Carbon cycle

Carbon dioxide is released into the atmosphere by volcanism, plant and animal respiration, and by fossil fuel burning. It is taken out of the atmosphere by photosynthesis, by dissolution into the ocean, and by weathering (dissolution into rain-drops which then react with silicate rocks on the continents). We will largely ignore the contributions to this cycle from the terrestrial biosphere (respiration and photosynthesis), and concentrate on the effects of weathering, fossil fuel emissions, and the interaction with the oceans. (The neglected components are in fact quite large, but we must restrict our scope).

Ignoring the ocean for the moment, conservation of atmospheric CO_2 can be expressed as

$$\frac{\mathrm{d}m_{\mathrm{CO_2}}}{\mathrm{d}t} = v - W, \tag{1.64}$$

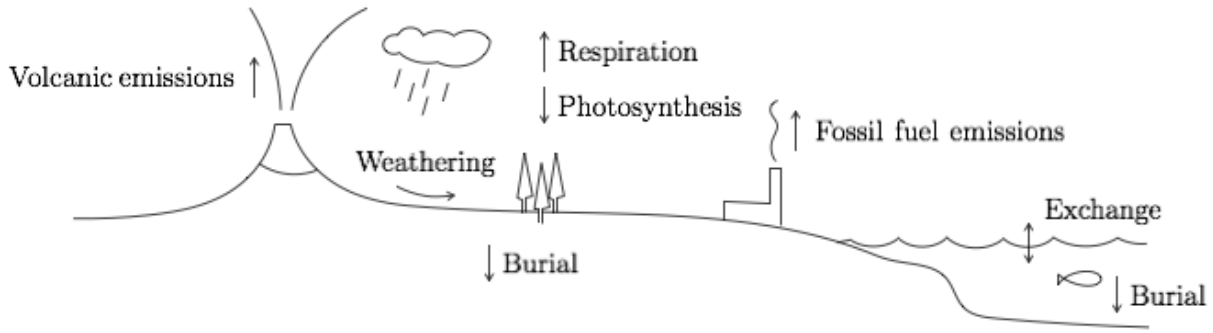

Figure 1.7: Components of the carbon cycle.

where m_{CO_2} is the total mass of CO_2 in the atmosphere, v represents emissions from volcanoes and from fossil fuel burning, W is the global weathering rate. It is convenient to express m_{CO_2} in terms of the atmospheric partial pressure p_{CO_2}, which we do using Dalton's law of partial pressures,

$$\frac{p_{CO_2}}{p_a} = \frac{m_{CO_2}}{m_a}\frac{M_a}{M_{CO_2}}, \tag{1.65}$$

(here $M_a = 29 \times 10^{-3}$ kg mol^{-1} and $M_{CO_2} = 44 \times 10^{-3}$ kg mol^{-1} are the molecular weights), and the fact that the atmospheric pressure is given by the hydrostatic balance $p_a A_E = m_a g$, where $A_E \approx 5.1 \times 10^{14}$ m^2 is the Earth's surface area. Thus

$$m_{CO_2} = \frac{A_E M_{CO_2}}{g M_a} p_{CO_2}. \tag{1.66}$$

The other common way of quantifying atmospheric CO_2 is as a concentration in parts per million (ppm). This is equivalent to the ratio $10^6(p_{CO_2}/p_a)$, and since $p_a \approx 10^5$ Pa, the concentration in ppm is approximately 10 times the partial pressure in Pa.

Volcanism provides an average flux of CO_2 to the atmosphere of around 0.3 Gt y^{-1} (1 Gt = 10^{12} kg). Current day CO_2 emissions from fossil fuels are around 30 Gt y^{-1} (although some of these emissions are offset by a corresponding increased dissolution in the oceans and photosynthesis). Note that we work in terms of CO_2 rather than C. Care is required with the units because emissions are often quoted in gigatons of carbon Gt(C), which can be converted to gigatons of CO_2 using the factor 44/12 (the ratio of molecular weights).

Weathering provides an important drawdown of CO_2 from the atmosphere. The CO_2 dissolves in rainwater and then reacts with calcium and magnesium silicates that are present in the Earth's crust. A principal reaction is

$$CaSiO_3 + 2CO_2 + H_2O \rightarrow SiO_2 + Ca^{2+} + 2HCO_3^-, \tag{1.67}$$

which converts calcium silicate and carbon dioxide to silica, calcium ions and bicarbonate ions. The calcium and bicarbonate ions then undergo a further reaction to produce calcium carbonate,

$$Ca^{2+} + 2HCO_3^- \rightarrow CaCO_3 + CO_2 + H_2O, \tag{1.68}$$

which is incorporated in the shells of marine organisms, and ultimately deposited as sediments on the sea floor or dissolved back into the deep ocean. The net effect of these reactions is

therefore to remove atmospheric CO_2 according to

$$CaSiO_3 + CO_2 \to CaCO_3 + SiO_2. \tag{1.69}$$

The rate of weathering therefore depends on temperature (which controls the pace of the weathering reactions), precipitation (which itself can be taken to depend on temperature, due to the approximate balance with evaporation), and the atmospheric concentration of carbon dioxide. Thus we may take the weathering rate $W = W(T, p_{CO_2})$, where the partial pressure p_{CO_2} is used as a measure of the atmospheric concentration of CO_2. An empirical relation is

$$W = W_0 \left(\frac{p_{CO_2}}{p_0} \right)^{\mu} \exp \left[\frac{T - T_0}{\Delta T_c} \right], \tag{1.70}$$

where $\mu = 0.3$, $\Delta T_c = 13$ K, and $T_0 = 288$ K, $p_0 = 36$ Pa, and $W_0 = 3 \times 10^{11}$ kg y^{-1} are estimated current-day values.

1.6.2 An energy and carbon balance model

Combining the ingredients above with the earlier energy balance model, and the description of ice-sheet albedo feedback, we have the following model

$$c\frac{\mathrm{d}T}{\mathrm{d}t} = \frac{1}{4}Q(1-a) - \sigma\gamma(p_{CO_2})T^4, \tag{1.71}$$

$$t_i\frac{\mathrm{d}a}{\mathrm{d}t} = a_0(T) - a, \tag{1.72}$$

$$\frac{A_E M_{CO_2}}{g M_a}\frac{\mathrm{d}p_{CO_2}}{\mathrm{d}t} = v - W(T, p_{CO_2}), \tag{1.73}$$

where $a_0(T)$ is given by (1.57), $W(T, p_{CO_2})$ is given by (1.70), and we have included a dependence of the greenhouse factor γ on p_{CO_2} so that we may investigate CO_2 driven feedbacks. For simplicity, this may be taken as a linear function

$$\gamma = \gamma_0 - \gamma_1 p_{CO_2}, \tag{1.74}$$

with $\gamma_0 = 0.64$, $\gamma_1 = 0.8 \times 10^{-3}$ Pa^{-1}.

The principle ingredient missing from this model is the transfer of CO_2 between atmosphere and ocean, which we will include below. However it is worth exploring the behaviour of this model before adding greater complexity.

We have a nonlinear dynamical system in the three variables T, a and p_{CO_2}. In fact, the timescale associated with (1.71) is very rapid, so we may treat the temperature as quasi-steady and reduce the system to a two-dimensional system, which can be analysed in the phase plane. In particular, we are interested in whether steady states exist, whether they are stable, and whether there are stable periodic orbits, which would perhaps correspond to the ice-age cycle.

We non-dimensionalise, writing

$$T = T_0 + \Delta T_c \hat{\theta}, \qquad p_{CO_2} = p_0 \hat{p}, \qquad t = t_i \hat{t}, \tag{1.75}$$

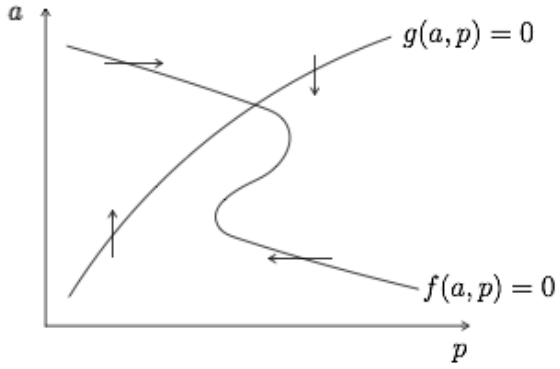

Figure 1.8: Phase plane for (1.82)-(1.83).

and defining dimensionless parameters

$$\varepsilon = \frac{c\Delta T_c}{t_i \sigma \gamma_0 T_0^4}, \quad \nu = \frac{4\Delta T_c}{T_0}, \quad q = \frac{Q}{4\sigma\gamma_0 T_0^4}, \quad \lambda = \frac{\gamma_1 p_0}{\gamma_0 \nu}, \quad \alpha = \frac{vgM_a t_i}{A_E p_0 M_{\mathrm{CO}_2}}, \quad w = \frac{W_0}{v}. \tag{1.76}$$

The model is then (dropping the hats),

$$\varepsilon \frac{\mathrm{d}\theta}{\mathrm{d}t} = q(1-a) - (1-\nu\lambda p)(1+\tfrac{1}{4}\nu\theta)^4, \tag{1.77}$$

$$\frac{\mathrm{d}a}{\mathrm{d}t} = B(\theta) - a, \tag{1.78}$$

$$\frac{\mathrm{d}p}{\mathrm{d}t} = \alpha(1 - wp^\mu e^\theta), \tag{1.79}$$

where $B(\theta)$ is the dimensionless version of the equilibrium albedo function. Using values given above, along with $c = 10^7$ J K^{-1} m^{-2}, $g = 9.8$ m s^{-2}, $t_i = 10^4$ y, $v = 3 \times 10^{11}$ kg y^{-1}, we find

$$\varepsilon \approx 1.6 \times 10^{-6} \quad \nu \approx 0.18 \quad q \approx 1.4, \quad \lambda \approx 0.25, \quad \alpha \approx 1.1, \quad w \approx 1. \tag{1.80}$$

The fact that $\alpha = O(1)$ indicates that the CO_2 partial pressure in this model varies on a similar (long) timescale to the albedo. Since $\varepsilon \ll 1$, the temperature rapidly approaches the quasi-steady state, which we expand to first order in ν,

$$\theta \approx \Theta(a,p) = \frac{q(1-a)-1}{\nu} + \lambda p. \tag{1.81}$$

We are left with a phase plane governed by

$$\dot{a} = f(a,p) = B(\Theta) - a, \tag{1.82}$$

$$\dot{p} = g(a,p) = \alpha(1 - wp^\mu e^\Theta). \tag{1.83}$$

Steady states occur at the intersection of the null clines of this system. The p nullcline is always an increasing function $a = G(p)$, whereas the a nullcline is either a decreasing function $a = F(p)$, or is a multivalued function of p, depending on the magnitude of the gradient of $B(\theta)$. In either case, there must be at least one possible steady state.

The stability of a steady state depends on the relative slopes of the nullclines at the intorsection point. If we perturb around a fixed point (p_0, a_0) by writing $(p, a) = (p_0, a_0) + (P, A)$ where P and A are small, then linearising gives

$$\begin{pmatrix} \dot{A} \\ P \end{pmatrix} = \begin{pmatrix} f_a & f_p \\ g_a & g_p \end{pmatrix} \begin{pmatrix} A \\ P \end{pmatrix}, \tag{1.84}$$

with the partial derivatives evaluated at the fixed point. There are exponential solutions,

$$\begin{pmatrix} A \\ P \end{pmatrix} \propto e^{\lambda t}, \tag{1.85}$$

where λ is are the eigenvalues of the matrix of partial derivatives. The steady state is stable if both eigenvalues have negative real parts, which happens if

$$T = f_a + g_p < 0, \qquad D = f_a g_p - f_p g_a > 0. \tag{1.86}$$

(T and D are the trace and determinant of the matrix). Moreover the approach to the fixed point is oscillatory (a spiral) if $D > \frac{1}{4}T^2$.

It can be shown (exercise) that if the steady state occurs on a section of the a nullcline where a is *increasing* with p, and if α is small enough, then the steady state is an unstable spiral. In this case there is instead a limit cycle, in which the trajectory orbits around the fixed point. If $\alpha \ll 1$, the limit cycle takes the form of a relaxation oscillator, moving rapidly onto the a nullcline ($\alpha \ll 1$ corresponds to the ice adjusting must faster than the CO_2).

1.6.3 Ocean carbon

We now turn attention to the role of carbon in the ocean. The ocean contains much more carbon than the atmosphere, and exchange between the atmosphere and ocean provides an important buffering to changes in atmospheric CO_2. To understand this requires considering more than just dissolved CO_2, however, because there is rapid exchange between different forms of carbon in the ocean.

We focus only on the inorganic carbon (*i.e.* that not contained in plants and animals and their remains), of which there are three main species: dissolved carbon dioxide CO_2, carbonate ions CO_3^{2-}, and bicarbonate ions HCO_3^-. We write the sum of these species as the total *dissolved inorganic carbon* (DIC),

$$C = [CO_2] + [CO_3^{2-}] + [HCO_3^-]. \tag{1.87}$$

Here the square brackets denote molar concentration, expressed as mol kg^{-1}.

We will shortly right down a conservation equation for this total carbon content, which includes the exchange with the atmosphere. However, we first discuss the partitioning between the different species. This partitioning is important because atmospheric CO_2 will evolve towards equilibrium with its dissolved concentration in the ocean, $[CO_2]$, so we need to know how that relates to the total carbon content. The majority ($\approx 90\%$) is currently held as bicarbonate ions, with less than 1% as CO_2.

The partitioning between the carbon species is described by the reactions

$$CO_2 + \left(H_2O\right) \underset{k_{-1}}{\overset{k_1}{\rightleftharpoons}} HCO_3^- + H^+, \tag{1.88}$$

$$HCO_3^- \underset{k_{-2}}{\overset{k_2}{\rightleftharpoons}} CO_3^{2-} + H^+. \tag{1.89}$$

The brackets on H_2O are to indicate that water molecules are so abundant that we can ignore their influence on the reaction rate. From these we can write down reaction rates using the

law of mass action,

$$R_1 = k_1[\mathrm{CO_2}] - k_{-1}[\mathrm{HCO_3^-}][\mathrm{H^+}], \tag{1.90}$$

$$R_2 = k_2[\mathrm{HCO_3^-}] - k_{-2}[\mathrm{CO_3^{2-}}][\mathrm{H^+}]. \tag{1.91}$$

These reactions are relatively rapid, so can be considered in equilibrium, *i.e.* $R_1 \approx 0$, $R_2 \approx 0$ (the reactions themselves equilibrate in a few minutes, but the rate-limiting process here is really associated with mixing in the ocean; we treat the ocean as a single well-mixed compartment, which is evidently a simplification). Thus

$$[\mathrm{HCO_3^-}][\mathrm{H^+}] = K_1[\mathrm{CO_2}], \tag{1.92}$$

$$[\mathrm{CO_3^{2-}}][\mathrm{H^+}] = K_2[\mathrm{HCO_3^-}], \tag{1.93}$$

where $K_1 = k_1/k_{-1} \approx 1.3 \times 10^{-6}$ mol kg^{-1}, and $K_2 = k_2/k_{-2} \approx 9.1 \times 10^{-10}$ mol kg^{-1} are the equilibrium constants (in general functions of temperature, though we will treat them as constants).

From this we see the important role also played by the hydrogen ions, which are directly related to the acidity of the ocean,

$$\mathrm{pH} = -\log_{10}[\mathrm{H^+}]. \tag{1.94}$$

The current pH of the ocean is around 8.2 (with $[\mathrm{H^+}] \approx 7 \times 10^{-9}$ mol kg^{-1}). If we assume the pH is known, the equilibrium conditions (1.92) and (1.93) provide two constraints on the concentrations of the three species $\mathrm{CO_2}$, $\mathrm{CO_3^{2-}}$, and $\mathrm{HCO_3^-}$. If we also suppose that we know the total carbon concentration (1.87), we can solve for the concentration of each. In particular

$$[\mathrm{CO_2}] = \frac{C}{1 + \frac{K_1}{[\mathrm{H^+}]} + \frac{K_1 K_2}{[\mathrm{H^+}]^2}}. \tag{1.95}$$

We will make use of this expression below. However there is no good reason to think that the pH should be fixed, and indeed it has been decreasing (a process referred to as ocean acidification). A better method to close the system is to consider the *alkalinity*. This is essentially a measure of charge balance, and it is (roughly) conserved. The total alkalinity includes contributions from many different compounds, but is dominated by the bicarbonate and carbonate ions. We thus define the alkalinity for our purpose as

$$A = 2[\mathrm{CO_3^{2-}}] + [\mathrm{HCO_3^-}], \tag{1.96}$$

and we suppose that this is fixed (the 2 is because there are two negative charges on the carbonate ion).

For a given total dissolved carbon content C and alkalinity A, we can use (1.87), (1.92), (1.93) and (1.96) to solve for all of $[\mathrm{CO_2}]$, $[\mathrm{CO_3^{2-}}]$, $[\mathrm{HCO_3^-}]$, and $[\mathrm{H^+}]$. Straightforward algebra leads to

$$[\mathrm{H^+}] = \frac{1}{2}(1-\gamma)K_1 \left[\left(1 + \frac{(2\gamma - 1)K_2}{(1-\gamma)^2 K_1} \right)^{1/2} - 1 \right], \tag{1.97}$$

where $\gamma = C/A \approx 0.85$ under present-day conditions. Since $K_2 \ll K_!$, this can be well approximated by

$$[\mathrm{H^+}] \approx \left(\frac{2\gamma - 1}{1 - \gamma} \right) K_2 = K_2 \frac{2C - A}{A - C}, \tag{1.98}$$

and hence

$$[\mathrm{HCO_3^-}] \approx 2C - A, \qquad [\mathrm{CO_3^{2-}}] \approx A - C, \qquad [\mathrm{CO_2}] \approx \frac{K_2}{K_1}\frac{(2C-A)^2}{A-C}, \tag{1.99}$$

More complicated models of the ocean chemistry take account of other ions, particularly calcium, and their effect on the alkalinity. In principle, one could attempt to model the concentrations of every species in the ocean, taking account of the sources and sinks (from weathering, precipitation, sedimentation etc.), but the model has to be closed at some stage in order to be manageable. Another common modification in more comprehensive models is to treat the surface and deep oceans as separate compartments.

Having established the partitioning between the different carbon species, we now return to the question of how the ocean carbon interacts with the atmosphere. For simplicity, we make use of (1.95) to relate the dissolved carbon dioxide to the total carbon content, effectively treating the pH as constant.

To describe the exchange with the atmosphere, we suppose that thermodynamic equilibrium holds at the ocean surface, and we parameterise the exchange of $\mathrm{CO_2}$ between the surface and the mixed layer of the ocean below. Thermodynamic equilibrium is described by Henry's law which relates the surface concentration $[\mathrm{CO_2}]_{surface}$ to the partial pressure in the atmosphere,

$$[\mathrm{CO_2}]_{surface} = K_H p_{\mathrm{CO_2}}, \tag{1.100}$$

where $K_H \approx 3.3 \times 10^{-7}$ mol kg^{-1} Pa^{-1} is the solubility (which decreases with increasing temperature). The exchange with the mixed layer is parameterised by

$$q = \tilde{h}\left([\mathrm{CO_2}]_{surface} - [\mathrm{CO_2}]\right), \tag{1.101}$$

where $\tilde{h}$ is an exchange coefficient, which is assumed constant (the exchange coefficient represents the effect of mixing in a narrow layer near the ocean surface, and in reality is likely to depend on factors such as wind speed). Putting these together, the $\mathrm{CO_2}$ flux from atmosphere to ocean is given by

$$q = h\left(p_{\mathrm{CO_2}} - \frac{C}{K}\right), \tag{1.102}$$

where we write $h = \tilde{h}K_H$, and $K = K_H(1 + K_1/[\mathrm{H^+}] + K_1K_2/[\mathrm{H^+}]^2)$, making use of (1.95). The units of h are kg Pa^{-1} s^{-1} so that the flux is a mass flux.

In addition, the weathering flux of $\mathrm{CO_2}$ transports carbon back into the ocean, so the sink term W in (1.64) should appear as a source term to the ocean.

Finally, we note that carbon is removed from the ocean by being incorporated into the shells of marine organisms, and then sedimenting to the ocean floor (a process referred to as the biological pump). We describe this using a simple exponential decay with rate constant b.

Thus, the overall ocean carbon budget is written as

$$\rho_O V_O \frac{\mathrm{d}C}{\mathrm{d}t} = \frac{h}{M_{\mathrm{CO_2}}}\left(p_{\mathrm{CO_2}} - \frac{C}{K}\right) + \frac{W}{M_{\mathrm{CO_2}}} - bC, \tag{1.103}$$

where ρ_O and V_O are the density and volume of the ocean, and $M_{\mathrm{CO_2}}$ is the molar mass, required as a conversion factor since C is the molar concentration.

1.6.4 An atmosphere and ocean carbon balance model

A simple model of the carbon cycle incorporating both atmosphere and ocean is now given by

$$\frac{A_E M_{\mathrm{CO}_2}}{g M_a} \frac{\mathrm{d}p_{\mathrm{CO}_2}}{\mathrm{d}t} = v - W - h\left(p_{\mathrm{CO}_2} - \frac{C}{K}\right), \tag{1.104}$$

$$\rho_O V_O \frac{\mathrm{d}C}{\mathrm{d}t} = \frac{h}{M_{\mathrm{CO}_2}}\left(p_{\mathrm{CO}_2} - \frac{C}{K}\right) + \frac{W}{M_{\mathrm{CO}_2}} - bC. \tag{1.105}$$

This can also be coupled with a model for the temperature and albedo, as in (1.71) and (1.72). For given emission v and weathering W, there is a steady state in which

$$C = \frac{v}{b}, \qquad p_{\mathrm{CO}_2} = \frac{C}{K} + \frac{v - W}{h}. \tag{1.106}$$

This state has a balance between emissions and sedimentation, and the atmospheric CO_2 is in equilibrium with the ocean. The timescale to achieve this equilibrium is large, of order $\rho_O V_O / b \sim 10^5$ y.

2 Rivers

2.1 Simple models and the flood hydrograph

2.1.1 Mass conservation

Rivers are usually much longer than their width or depth, and are therefore modelled as quasi-one-dimensional features, described by the discharge (flux) Q ($\mathrm{m}^3\ \mathrm{s}^{-1}$), and cross-sectional area A (m^2). The essential ingredient is conservation of mass, expressed by

$$\frac{\partial A}{\partial t} + \frac{\partial Q}{\partial x} = E, \tag{2.1}$$

where s is distance downstream, t is time, and E ($\mathrm{m}^2\ \mathrm{s}^{-1}$) is a source term, describing precipitation, runoff, and flow from tributaries.

This equation can be derived in a number of different ways. Consider a small section of the river between x_1 and x_2. The rate of change of the volume of water in the region is

$$\frac{\mathrm{d}}{\mathrm{d}t}\int_{x_1}^{x_2} A\ \mathrm{d}x = Q_1 - Q_2 + \int_{x_1}^{x_2} E\ \mathrm{d}x, \tag{2.2}$$

Using the fundamental theorem of calculus, we can write this as

$$\int_{x_1}^{x_2} \frac{\partial A}{\partial t}\ \mathrm{d}x = \int_{x_1}^{x_2} -\frac{\partial Q}{\partial x} + E\ \mathrm{d}x. \tag{2.3}$$

This holds for any x_1 and x_2 and therefore, assuming A and Q are continuously differentiable, we obtain (2.1).

2.1.2 Turbulent flow

To relate the discharge to the cross-sectional area we must consider the fluid mechanics. The flow in a river is typically turbulent, involving chaotic trajectories with velocity varying rapidly in time and space. This means it is not well described by either the inviscid or laminar viscous

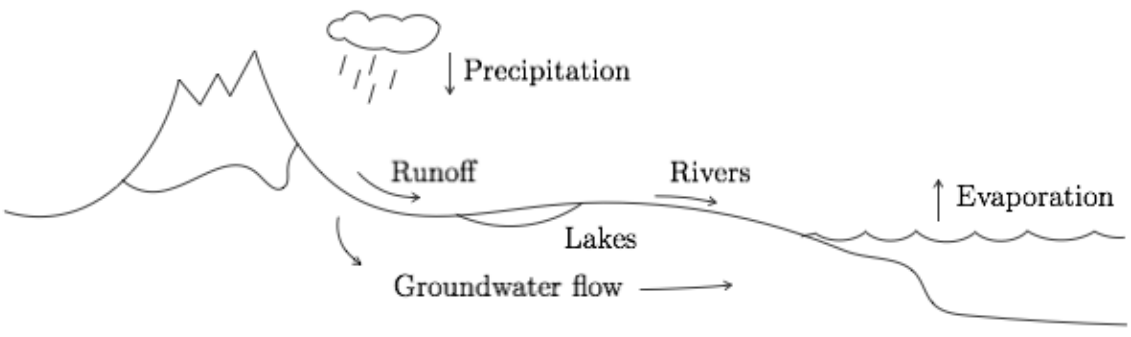

Figure 2.1: Components of the hydrological cycle.

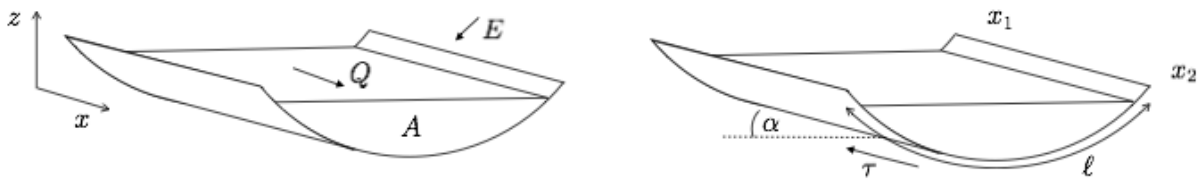

Figure 2.2: Cross-section of a river.

.

fluid theory that may be familiar. Turbulent flow occurs when the Reynolds number, which is a dimensionless measure of the flow speed, is larger than a critical value $Re_c \approx 10^3$ (the precise value depends on the situation). The Reynolds number is defined by

$$Re = \frac{[u][h]}{\nu}, \tag{2.4}$$

where $\nu \approx 10^{-6}$ m^2 s^{-1} is the kinematic viscosity of water, and $[u]$ and $[h]$ are the scales for flow speed and depth.

We can describe the turbulent flow using the average downstream velocity $u = Q/A$, and a parameterisation of the drag force that the fluid exerts on the walls of the channel. A common parameterisation of this drag force is

$$\tau = f\rho u^2, \tag{2.5}$$

where $f \approx 0.01$ is a friction factor, ρ is the density, and u is the average flow speed.

2.1.3 Force balance

We assume the flow is slowly varying, which allows us to neglect accelerations. The force balance within a cross-section is then

$$\tau\ell = \rho g S A, \tag{2.6}$$

where τ is the wall shear stress acting over wetting perimeter ℓ, ρ is the density, g is the gravitational acceleration, $S = \sin\alpha$ is the slope, and A is the cross-sectional area. The left hand side is the force per unit length resisting the flow, and the right hand side is the component of weight per unit length in the downstream direction.

Using the parameterisation for shear stress (2.5), this gives

$$u = CR^{1/2}S^{1/2}, \tag{2.7}$$

where we define $C = (g/f)^{1/2}$, and the hydraulic radius

$$R = \frac{A}{\ell}. \tag{2.8}$$

This is referred to as the *Chèzy law*, and the constant C as the Chèzy coefficient (Chèzy, 1775).

An alternative empirical description of flow in an open channel that is commonly used is the *Manning law*,

$$u = \frac{R^{2/3}S^{1/2}}{n}, \tag{2.9}$$

where $n' \approx 0.01 - 0.1$ m$^{-1/3}$ s is the Manning coefficient (Manning, 1890). This is equivalent to a shear stress parameterisation

$$\tau = \frac{\rho g n^2 u^2}{R^{1/3}}, \tag{2.10}$$

and we can therefore identify f with $gn^2/R^{1/3}$, or $C = R^{1/6}/n$.

Either (2.7) or (2.9) can be combined with the definition of flux $Q = uA$, to provide a relationship between discharge and cross-sectional area.

The relationship includes the hydraulic-radius, which itself can be related to the cross-sectional area with an assumption about the geometry of the cross-section. For a canal-shaped cross-section of given width w and smaller height h, we have $A = wh$, and $\ell = w + 2h \approx w$, so that $R = A/\ell \approx A/w = h$. For a notch-shaped cross-section with lateral slope angle β, we have $A = \frac{1}{8}\ell^2 \sin 2\theta$, so $R = A/\ell = A^{1/2}\left(\frac{1}{8}\sin 2\theta\right)^{1/2}$.

In all cases, we can therefore write

$$Q = \frac{cA^{m+1}}{m+1}, \tag{2.11}$$

where, for the Chézy law, $m + 1 = 3/2$ for a canal-shape and $m + 1 = 5/4$ for a notch or circular shaped cross-section, and for the Manning law, $m + 1 = 5/3$ or $4/3$.

2.1.4 Characteristics and shocks

Putting the relationship (2.11) together with the mass conservation equation (2.1) we have

$$\frac{\partial A}{\partial t} + cA^m \frac{\partial A}{\partial x} = E. \tag{2.12}$$

This is a first order quasi-linear equation, and can be solved using the method of characteristics. Since it is non-linear, solutions will generically form shocks (discontinuities), discussed below.

As an example, consider solving the equation on an infinite domain, with no source, and with initial condition $A = A_0(x)$ (the water is assumed to have come from a previous storm, say, or from far upstream). The characteristic equations are

$$\frac{\mathrm{d}t}{\mathrm{d}\tau} = 1, \qquad \frac{\mathrm{d}x}{\mathrm{d}\tau} = cA^m, \qquad \frac{\mathrm{d}A}{\mathrm{d}\tau} = 0, \tag{2.13}$$

with initial conditions,

$$t = 0, \qquad x = \sigma, \qquad A = A_0(\sigma), \qquad \text{at} \quad \tau = 0. \tag{2.14}$$

Here τ is used as the variable parameterising each characteristic, and σ is used as the variable parameterising the initial data. We see immediately that $t = \tau$, as is common for this type of equation, and therefore we could just as well take t as the variable parameterising the characteristics.

We also see that $A = A_0(\sigma)$ is constant along each characteristic, which are therefore given by

$$x = \sigma + cA_0(\sigma)^m t, \tag{2.15}$$

and this implicitly defines the solution as

$$A(x, t) = A_0(x - cA^m t). \tag{2.16}$$

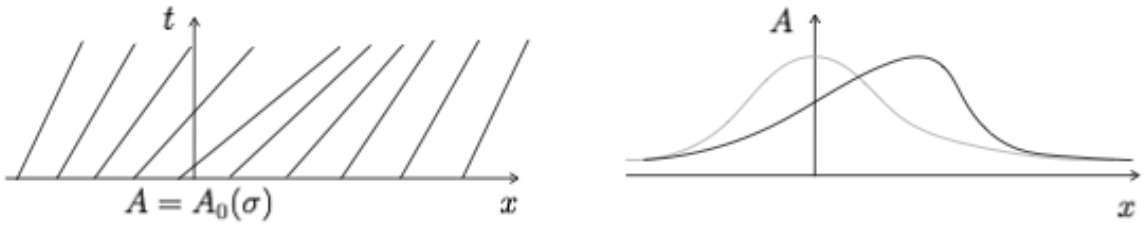

Figure 2.3: (a) Characteristic diagram and (b) cross-sectional area A at $t = 0$ and some later time.

So the initial cross-sectional profile is advected downstream at a speed that depends upon the profile. Larger areas move faster, and this generically leads to the formation of shocks (discontinuities).

Shocks must be described by interpreting the equation in weak form or (equivalently) by returning to the conservation arguments from which the equation was derived. In the frame of a shock moving with speed $\dot{x}_s$, the discharge into and out of the shock must balance, so

$$Q_- - A_-\dot{x}_s = Q_+ - A_+\dot{x}_s, \tag{2.17}$$

where $-$ and $+$ denote upstream and downstream of the shock. Thus

$$\dot{x}_s = \frac{[Q]^+_-}{[A]^+_-} = \frac{Q_+ - Q_-}{A_+ - A_-}. \tag{2.18}$$

We can find when a shock will form either by looking for where neighbouring characteristics intersect, or by looking for where the gradient of the solution $|\partial A/\partial x|$ becomes infinite. Differentiating (2.16) implicitly gives

$$A_x = A_0'(\sigma)\left(1 - mctA^{m-1}A_x\right), \tag{2.19}$$

and therefore

$$A_x = \frac{A_0'}{1 + mctA_0^{m-1}A_0'}, \tag{2.20}$$

which blows up (tends towards $-\infty$) as $t \to -1/mcA^{m-1}A_0'$. This will happen at different times for different σ (provided $A_0'(\sigma)$ is negative), but we are interested in the first time at which it occurs, which is

$$t_s = \min_{A_0'(\sigma)<0}\left(-\frac{1}{mcA_0^{m-1}A_0'}\right). \tag{2.21}$$

After this moment, a shock must be inserted into the solution. The characteristic equations still hold on either side, but must not be continued through the shock, which moves according to (2.18).

2.1.5 Flood hydrograph

We want to understand how the water level in a river will vary during the course of a flood. We consider the case of a localised storm at $x = 0$, which can be modelled using the initial condition $A(x, 0) = V_0\delta(x)$, where $\delta(x)$ is the delta function.

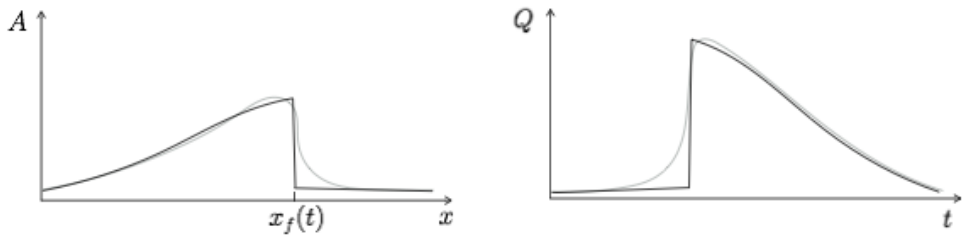

Figure 2.4: Propagation of a flood wave, and corresponding flood hydrograph. Grey lines show the smoothing effect of including the pressure gradient in the St Venant equations.

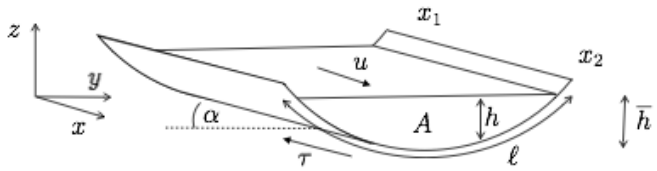

Figure 2.5: Force balance on a segment of a river.

.

This will immediately produce a shock that moves downstream. Indeed from the general solution (2.16) we see that $A = 0$ unless $x = cA^m t$, and the solution is therefore

$$A = 0 \qquad x > x_f, \tag{2.22}$$

$$A = (x/ct)^{1/m} \quad 0 < x < x_f, \tag{2.23}$$

where the front x_f moves according to

$$\dot{x}_f = \frac{Q_-}{A_-} = \frac{cA_-^m}{m+1} = \frac{1}{m+1}\frac{x_f}{t}. \tag{2.24}$$

Hence $x_f = Ct^{1/(m+1)}$, and the constant C is determined from the global mass constraint

$$\int_0^{x_f} A \, \mathrm{d}x = V_0, \tag{2.25}$$

which gives

$$C = \left(\frac{m+1}{m}\right)^{m/(m+1)} c^{1/(m+1)} V_0^{m/(m+1)}. \tag{2.26}$$

2.2 St Venant equations

2.2.1 Force balance

We now consider cases where the acceleration of the water is non negligible. We will see that the magnitude of the acceleration terms is described by a dimensionless number called the *Froude number*, which is a measure of how 'rapid' a river is.

Consider a section of the river between x_1 and x_2. Conservation of momentum (ρAu) can be expressed by

$$\frac{\mathrm{d}}{\mathrm{d}t}\int_{x_1}^{x_2} \rho Au \,\mathrm{d}x = -\left[\rho Au^2\right]_{x_1}^{x_2} + \int_{x_1}^{x_2} \rho gAS - \tau\ell \,\mathrm{d}x - \left[\overline{p}A\right]_{x_1}^{x_2}, \tag{2.27}$$

where the terms on the right are the net momentum flux into this section of the river, the gravitational and frictional forces (which were previously assumed to be the only important components of this balance), and the net pressure force. We ignore any runoff and tributaries, which would provide additional source terms on the right hand side. Using the fundamental theorem of calculus, and assuming A and u are continuously differentiable, we derive

$$\frac{\partial}{\partial t}(\rho Au) + \frac{\partial}{\partial x}(\rho Au^2) = \rho gAS - \tau\ell - \frac{\partial}{\partial x}(\overline{p}A). \tag{2.28}$$

Together with the mass conservation equation

$$\frac{\partial}{\partial t}(\rho A) + \frac{\partial}{\partial x}(\rho Au) = 0, \tag{2.29}$$

these are referred to as the *St Venant equations*.

The equations are not yet closed, because we must prescribe a parameterisation for the shear stress τ, and establish how the wetted perimeter ℓ and average pressure $\overline{p}$ depend on the cross-sectional area.

For the average pressure, we assume that the pressure is hydrostatic, so $p = \rho g(\eta - z)$, where $\eta(x,t)$ is the elevation of the water surface (assumed to be independent of the cross-stream coordinate y). Then the average pressure is defined by

$$\overline{p}A = \int_{y_l}^{y_r}\int_{b}^{\eta} \rho g(\eta - z)\,\mathrm{d}z\,\mathrm{d}y, \tag{2.30}$$

where $b(y)$ is the bed elevation and the integral is taken over the whole cross section from the left bank at y_l to the right bank at y_r. We can write this as

$$\overline{p}A = \int_{y_l}^{y_r} \frac{1}{2}\rho g h^2 \,\mathrm{d}y, \tag{2.31}$$

where $h(x,y,t) = \eta(x,t) - b(y)$ is the depth, which might vary with the transverse coordinate y, depending on the cross-sectional geometry. Regardless of the geometry,

$$\frac{\partial}{\partial x}(\overline{p}A) = \int_{y_l}^{y_r} \rho g h\frac{\partial h}{\partial x}\,\mathrm{d}y = \rho gA\frac{\partial \eta}{\partial x} = \rho gA\frac{\partial \overline{h}}{\partial x}, \tag{2.32}$$

where we have taken $\overline{h} = \eta - \overline{b}$ as the mean depth across the cross section.

Rearranging (2.28), making use of (2.29), we find

$$\frac{\partial u}{\partial t} + u\frac{\partial u}{\partial x} = gS - \frac{\tau\ell}{\rho A} - g\frac{\partial \overline{h}}{\partial x}. \tag{2.33}$$

We concentrate on the case of a canal of width w, so $\overline{h} = A/w$ and $\ell \approx w$. We also adopt the shear stress description $\tau = f\rho u^2$ from (2.5) and which leads to Chézy's law under steady conditions. In this case

$$\frac{\tau\ell}{\rho A} = \frac{fwu^2}{A}, \qquad g\frac{\partial \overline{h}}{\partial x} = \frac{g}{w}\frac{\partial A}{\partial x}, \tag{2.34}$$

so the equations become

$$\frac{\partial A}{\partial t} + \frac{\partial}{\partial x}(Au) = 0. \tag{2.35}$$

$$\frac{\partial u}{\partial t} + u\frac{\partial u}{\partial x} = gS - \frac{fwu^2}{A} - \frac{g}{w}\frac{\partial A}{\partial x}. \tag{2.36}$$

2.2.2 Non-dimensionalisation

We scale

$$x = [x]\hat{x}, \quad t = [t]\hat{t}, \quad A = [A]\hat{A}, \quad u = [u]\hat{u}, \tag{2.37}$$

and suppose the length scale $[x]$ is given, choosing other scales so that

$$[t] = \frac{[x]}{[u]}, \quad [A][u] = Q_0, \quad gS[A] = fw[u]^2. \tag{2.38}$$

Here Q_0 is a given discharge scale. It is common when studying rivers to suppose that this scale is known (for any given river we wish to study we could measure or estimate it); this informs the model of how large a river we are dealing with. The choice of timescale is the natural 'advective' timescale. The balance between gravity and friction force is motivated by the fact that this must be the balance under uniform and steady conditions. Rearranging these constraints on the scales, we have

$$[u] = \left(\frac{gSQ_0}{fw}\right)^{1/3}, \quad [A] = \left(\frac{fwQ_0^2}{gS}\right)^{1/3}. \tag{2.39}$$

For example, for the Thames at Oxford we might take $Q_0 = 20$ m^3 s^{-1}, $w = 10$ m, $f = 0.05$, $g = 10$ m s^{-2}, $S = 10^{-3}$, then $[u] = 0.7$ m s^{-1}, and $[A] = 27$ m^2.

The dimensionless equations become

$$\frac{\partial A}{\partial t} + \frac{\partial}{\partial x}(Au) = 0, \tag{2.40}$$

$$\delta F^2\left(\frac{\partial u}{\partial t} + u\frac{\partial u}{\partial x}\right) = 1 - \frac{u^2}{A} - \delta\frac{\partial A}{\partial x}. \tag{2.41}$$

The dimensionless numbers are the Froude number,

$$F = \frac{[u]}{\sqrt{g[h]}}, \tag{2.42}$$

where $[h] = [A]/w$ is the depth scale, and the ratio of the depth gradient to bed slope,

$$\delta = \frac{[h]}{S[x]}. \tag{2.43}$$

The Froude number is a measure of how rapid the river is. Note that $\sqrt{gh}$ is the speed of surface waves on a layer of water of depth h, so the Froude number can be thought of as the ratio of the river speed to the speed of surface waves. This will have relevance below for the direction of propagation of surface waves on a river. If $F > 1$ the river flow is referred to as *supercritical*, whereas is $F < 1$ it is *subcritical*.

Note that it would be possible to choose the length scale $[x]$ so as to make $\delta = 1$. This would define a natural length scale on which the pressure gradients are comparable with the gravitational term and the shear stress. However, we usually imagine that an external length scale is imposed on the problem (for instance, we are interested in predicting flood conditions at certain locations).

2.2.3 Limits

The equations (2.40) and (2.41) are a pair of first order nonlinear hyperbolic equations. They can again be solved using the method of characteristics, although doing so analytically is not possible in general. Below we will consider steady states and linearised perturbations to the steady states. First, we note how the equations behave under certain limits.

In the limit $\delta \ll 0$ (long-wave theory), we recover the slowly varying model from earlier, since the force balance equation reduces to $u^2 \approx A$, and therefore $Q = Au = A^{3/2}$. If in addition $F \ll 1$ (the flow is sufficiently tranquil), then the approximation can be improved to give

$$u^2 \approx A\left(1 - \delta\frac{\partial A}{\partial x}\right). \tag{2.44}$$

Substituting this into the mass equation gives

$$\frac{\partial A}{\partial t} + \tfrac{3}{2}A^{1/2}\frac{\partial A}{\partial x} = \tfrac{1}{2}\delta\frac{\partial}{\partial x}\left(A^{3/2}\frac{\partial A}{\partial x}\right), \tag{2.45}$$

so the correction provides a non-linear diffusion term. This has the effect of smoothing out (regularising) the shocks that would form in the absence of the diffusion term. If $0 < \delta \ll 1$, the effect on the flood hydrograph is to provide a sharply rising curve, rather than a discontinuous jump up as in the case of $\delta = 0$.

If $\delta \gg 1$ (i.e. the length scale of consideration is sufficiently short), the momentum equation can be approximated as

$$F^2\left(\frac{\partial u}{\partial t} + u\frac{\partial u}{\partial x}\right) + \frac{\partial A}{\partial x} = 0, \tag{2.46}$$

which together with the mass equation (2.40) are the *shallow water equations*. These apply when we consider short length scales, or very shallow hill slopes, so that the downstream component of gravity and friction play a negligible role.

2.2.4 Stability

Consider the dimensionless model for the canal (since cross-section A and depth h are linearly related we can use either as the primary variable),

$$\frac{\partial h}{\partial t} + \frac{\partial}{\partial x}(hu) = 0, \tag{2.47}$$

$$F^2\left(\frac{\partial u}{\partial t} + u\frac{\partial u}{\partial x}\right) = 1 - \frac{u^2}{h} - \frac{\partial h}{\partial x}. \tag{2.48}$$

We have chosen the length scale so that $\delta = 1$.

There is a uniform steady state with $u^2 = h$ and $uh = 1$ (by the choice of the non-dimensionalisation we can set the dimensionless flux uh to 1 without loss of generality). Thus $u = h = 1$.

We consider the linear stability of this uniform state by writing $u = 1 + U$, $h = 1 + H$, where the capitalised variables will be supposed small. Substituting into the equations gives

$$H_t + H_x + U_x = 0, \tag{2.49}$$

$$F^2(U_t + U_x) = -2U + H - H_x, \tag{2.50}$$

which we can rearrange into

$$F^2\left(\frac{\partial}{\partial t} + \frac{\partial}{\partial x}\right)^2 U = -2\left(\frac{\partial}{\partial t} + \frac{\partial}{\partial x}\right) U - \frac{\partial U}{\partial x} + \frac{\partial^2 U}{\partial x^2}. \tag{2.51}$$

As usual with linear stability analyses, we look for exponential solutions,

$$U = \hat{U}\exp((\sigma t + ikx)/F^2) = \hat{U}\exp((\sigma_R t + i(kx + \sigma_I t))/F^2), \tag{2.52}$$

where we write $\sigma = \sigma_R + i\sigma_I$, and where σ_R/F^2 is the growth rate, k/F^2 is the wave number, and $-\sigma_I/k$ is the wave speed (the factors of F^2 are included in the exponential with hindsight, to make the algebra easier).

Substituting into the equation we obtain the dispersion relation

$$\sigma = -1 - ik + \left(1 - ik - \frac{k^2}{F^2}\right)^{1/2}, \tag{2.53}$$

which is most easily analysed by writing the square root as $p - iq$, say, so that

$$\sigma_R = -1 \pm p, \qquad -\frac{\sigma_I}{k} = 1 \pm \frac{q}{k}, \tag{2.54}$$

(we may take $p > 0$ without loss of generality). By the definition of $p - iq$, equating real and imaginary parts,

$$2pq = k, \qquad p^2 - q^2 = 1 - \frac{k^2}{F^2}, \tag{2.55}$$

and so

$$L(p) := p^2 - \frac{k^2}{4p^2} = 1 - \frac{k^2}{F^2}. \tag{2.56}$$

The left hand side here is an increasing function of p, so $p > 1$ (which leads to $\sigma_R > 0$ and therefore instability) if and only if $L(p) > L(1)$, *i.e.* if and only if

$$1 - \frac{k^2}{F^2} > 1 - \frac{k^2}{4}, \tag{2.57}$$

which requires $F > 2$. Thus surface waves are unstable if the flow is sufficiently fast.

The wave speeds are of opposite sign (*i.e.* one moves upstream and the other downstream) unless $q < k$, which is the case if and only if $p > \frac{1}{2}$, or equivalently $L(p) > L(\frac{1}{2})$. This requires

$$1 - \frac{k^2}{F^2} > \frac{1}{4} - k^2, \tag{2.58}$$

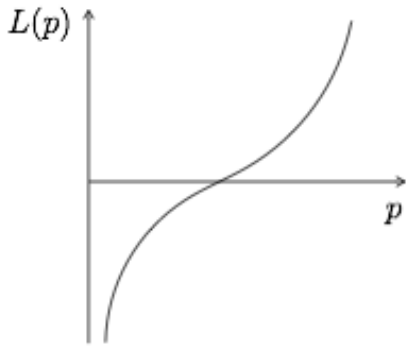

Figure 2.6: The function $L(p)$ defined in (2.56).

or equivalently

$$\frac{3}{4} > k^2 \left(\frac{1}{F^2} - 1 \right). \tag{2.59}$$

Thus for $F > 1$, all waves travel downstream, and the flow is described as super-critical (although if $F < 2$ the waves are stable and will decay as they travel). For $F < 1$, waves can travel both up and downstream and the flow is described as subcritical (although waves with small enough wavenumber will all travel downstream even in this case).

In the case $F > 2$, the instability evolves to produce non-linear waves, referred to as *roll waves*. These are often visible in heavy rain on steep pavement. They form periodic trains of waves that can be analysed by looking for travelling wave type solutions of the equations $A = A(x - ct)$, $u = u(x - ct)$.

2.3 Sediment transport and Dunes

This section concerns the erosion and transport of sediment in rivers, and the resultant sculpting of the river bed to form *dunes* and *anti-dunes*. We focus on rivers, but many of the ideas are also relevant to subaerial erosion and transport (driven by the wind, rather than by water flow), and therefore to the formation of a larger class of landforms, including desert sand-dunes.

2.3.1 Patterns in rivers

Erosion and sediment transport are responsible for may different patterns in rivers. On a large scale, the path of the river channel is a result of the long-term interaction with the substrate (which may be rigid bedrock, or may be looser sediments that were deposited previously by floods, wind, or by deglaciation). *Meanders* are the most obvious manifestation of this patterning. These are associated with a secondary transverse flow that results in larger velocities and hence more erosion on the outer banks of bends. Although we will not discuss meandering further, there is a large and interesting literature on the mechanisms that lead to it.

In a river channel itself, there are several types of instability that can occur to the uniform flow state. The basic mechanism for instability is that erosion rates typically increases with water speed, which increases with water depth. Thus deeper areas undergo more erosion, and this provides a positive feedback. Instabilities can be broadly classified according to whether the bed profile variations are transverse or parallel to flow.

Figure 2.7: Meanders and lateral bars.

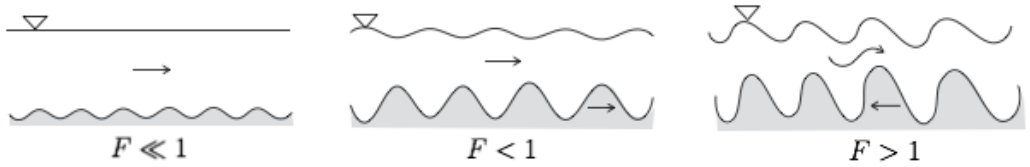

Figure 2.8: Ripples, dunes, and anti-dunes.

Transverse instabilities produce *lateral bars*. Such bars commonly form in gravel-bedded rivers, and often interact with a meandering instability to form alternating bars, on alternate sides of the river. In wide rivers, many bars may form across the channel and are referred to as multiple row bars. They often form when the river is high, and produce islands or beaches when the water level drops. For much of the time such rivers are split into many connecting braids, and are referred to as a *braided river*. Vegetation may form on the bars, and helps to stabilise them against further erosion.

Longitudinal instabilities have undulations in the downstream direction, and are referred to as ripples, dunes or anti-dunes. Which of these occurs depends on the flow conditions, and particularly on the size of the Froude number F. Dunes form at low Froude number ($F < 1$); they move slowly downstream, are typically of small amplitude compared to the depth of the river, and have river surface perturbations that are out of phase with the bed. Anti-dunes form at high Froude numbers ($F > 1$); they move upstream and have large amplitude surface perturbations that are in phase with those in the bed. Anti-dunes are often seen on shallow streams flowing over a beach.

We will primarily focus on understanding the mechanism for these longitudinal instabilities, and we will restrict attention to their linear (small amplitude) evolution. Much of the erosion of river channels occurs during floods, when the river channel is at its widest and the erosive power of the flow is greatest. Nevertheless, we will restrict our attention to steady flow conditions.

The mechanisms responsible for forming *aeolian* dunes are similar to those considered here, but the fact that the wind can change direction more easily than a river gives rise to a larger range of behaviour. Similar 'transverse' dunes do occur, at right angles to a strongly prevailing wind direction. They typically have a distinctive sharp crest, which is due to separation of the flow at this point to form a recirculating pocket on the lee side of the dune. This causes the upstream side to have a relatively shallow slope, and the downstream side to have a steep slope (typically at the limiting angle of friction).

Linear dunes can also form aligned with the mean wind direction, if two different prevailing

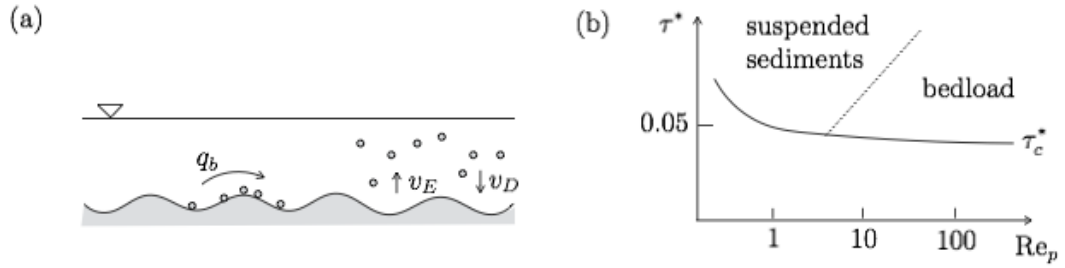

Figure 2.9: (a) Bedload transport and suspended sediment, and (b) critical Shields stress τ^* for sediment transport as a function of particle Reynolds number Re_p.

directions alternately blow from each side of the dune; these are called seifs. Star-shaped dunes form when the wind blows from many different directions. Another common aeolian dune is the barchan dune, which has a crescent shape with the arms pointing in the direction of the wind. These typically form when there is a limited supply of sand. Anti-dunes do not form in the desert because the effective Froude number is not large enough.

2.3.2 Sediment transport mechanisms

Sediment transport occurs by two processes: *bedload* and *suspension*. For given flow conditions, larger particles will roll along the bed, dragged by the stress exerted by the fluid. This is the bedload transport. Smaller particles are entrained by turbulent eddies into the flow to be transported in suspension. Suspended particles also settle out of the water, due to their greater density, and a steady-state balance between entrainment and deposition determines the suspended sediment load.

Natural rivers have a large range of grain sizes: gravel is typically > 1 mm, sand in the range $60\ \mu\text{m} - 1$ mm, silt in the range $2 - 60\ \mu$m. Sufficiently large particles can be neither entrained nor dragged along the bed, and are essentially immobile. Empirical observations suggest that a dimensionless measure of the basal shear stress, referred to as the Shields stress, is a good indicator of whether given grains will be mobilised under a given shear stress. The Shields stress is defined by

$$\tau^* = \frac{\tau}{\Delta\rho g D_s}, \tag{2.60}$$

where τ is the shear stress, D_s is the grain size, and g the gravitational acceleration, and $\Delta\rho = \rho_s - \rho_w$ the density difference between the grain and water. Sediment transport occurs if τ^* is larger than a critical value τ_c^*, which itself depends on the particle size via the particle Reynolds number

$$Re_p = \frac{u_* D_s}{\nu_w}, \tag{2.61}$$

where $\nu_w \approx 10^{-6}$ m^2 s^{-1} is the kinematic viscosity of water, and u_* is the *friction velocity*, defined by

$$u_* = (\tau/\rho_w)^{1/2}. \tag{2.62}$$

The dependence of τ_c^* on Re_p is relatively weak ($\tau_c^* \approx 0.06$ except at low low rates). Above τ_c^*, sediment transport occurs by suspension (at low Re_p) or bedload (at high Re_p).

The shear stress can be related to the mean flow using the law (2.5),

$$\tau = f\rho_w u^2, \tag{2.63}$$

where f is a dimensionless friction factor in the range $0.01 - 0.1$ (in this case $u_* = f^{1/2}u$).

Descriptions for bedload transport and for erosion are ultimately empirical.

Bedload is described in terms of a bedload flux q_b, with units $\mathrm{m}^2\ \mathrm{s}^{-1}$ (the volume transported per unit stream width per unit time). This is typically a function of the basal shear stress, and therefore of the stream speed, through (2.63). One common description is the Meyer-Peter-Müller relation,

$$q_b = (\Delta\rho g D_s^3/\rho_w)^{1/2} q_*, \qquad q_* = K\left[\tau^* - \tau_c^*\right]_+^{3/2}. \tag{2.64}$$

Here q_* is a dimensionless bedload flux, with $\tau_c^* \approx 0.047$ the threshold Shields parameter defined above, $K \approx 8$ a dimensionless constant, and $[\cdot]_+ = \max(\cdot, 0)$.

Suspended sediment is described in terms of the concentration c of sediment in the water column (there is a choice of units for concentration; we use $\mathrm{kg\ m}^{-3}$). Erosion from the bed (or entrainment of previously eroded sediments) is described using an erosion rate v_E (with units $\mathrm{m\ s}^{-1}$), which is, like bedload, empirical function of the shear stress. Deposition occurs at a rate v_D that is proportional to the concentration of sediments, and to their settling velocity. The latter is a function of the particle size and density (it is referred to as Stokes settling velocity and can be derived using Stokes equations for low-Reynolds number flow),

$$v_s = \frac{\Delta\rho g D_s^2}{18\eta_w}. \tag{2.65}$$

We use this velocity scale to non-dimensionalise the erosion and deposition rates, writing

$$v_E = v_s E, \qquad v_D = v_s \frac{c}{\rho_s}, \tag{2.66}$$

where E is a dimensionless function of shear stress τ or velocity u.

2.3.3 Exner equation and suspended sediment concentration

We consider a two-dimensional river (e.g. a wide canal), with bed elevation $s(x,t)$, depth $h(x,t)$, and surface elevation $\eta = s + h$. The essential equation describing bedform evolution is the Exner equation,

$$(1-n)\frac{\partial s}{\partial t} + \frac{\partial q_b}{\partial x} = v_D - v_E. \tag{2.67}$$

This equation represents conservation of sediment in the bed; n is the bed porosity (assumed constant). The deposition and erosion terms on the right hand side represent a source and sink of sediment, which is passed into suspension. These appear as equal and opposite source terms in the equation for suspended sediment conservation

$$\frac{\partial}{\partial t}(hc) + \frac{\partial}{\partial x}(huc) = \rho_s(v_E - v_D), \tag{2.68}$$

Using mass conservation of the fluid this can also be written

$$h\frac{\partial c}{\partial t} + hu\frac{\partial c}{\partial x} = \rho_s(v_E - v_D). \tag{2.69}$$

2.3.4 Bedload transport

We consider first the evolution of a bed accounting only for bedload transport, so $v_E = v_D = 0$. Our aim is to establish under what conditions, if any, we can explain the formation of dunes or anti-dunes. We must combine the Exner equation (2.67) with an empirical law for the bedload flux $q_b(\tau)$, and a description of the fluid flow.

For the fluid flow, we adopt the St Venant equations in the form

$$\frac{\partial h}{\partial t} + \frac{\partial}{\partial x}(hu) = 0, \tag{2.70}$$

$$\frac{\partial u}{\partial t} + u\frac{\partial u}{\partial x} = g\left(S - \frac{\partial \eta}{\partial x}\right) - \frac{fu^2}{h}, \tag{2.71}$$

appropriate for a wide canal with depth h, and where we have used the parameterisation $\tau = f\rho u^2$. This is combined with the Exner equation, which we write in the form

$$(1-n)\frac{\partial s}{\partial t} + \frac{\partial q_b}{\partial x} = 0. \tag{2.72}$$

There are two timescales at play here, and the situation is simplified by the fact that these are typically quite different, the timescale for bedload transport being much longer than the advective timescale for the flow. This is made clear by non-dimensionalising the model.

We write

$$x = [x]\hat{x}, \quad t = [t]\hat{t}, \quad u = [u]\hat{u}, \quad s, h, \eta = [h]\left(\hat{s}, \hat{h}, \hat{\eta}\right), \quad q_b = [q_b]\hat{q}. \tag{2.73}$$

The balance of terms in the momentum equation suggests we choose scales so that

$$gS[h] = f[u]^2, \tag{2.74}$$

and we take the flux scale $Q = [h][u]$ as given, so choose scales

$$[h] = \left(\frac{fQ^2}{gS}\right)^{1/3}, \quad [u] = \left(\frac{gSQ}{f}\right)^{1/3}, \quad [t] = \frac{(1-n)[h][x]}{[q_b]}. \tag{2.75}$$

It is possible to choose the length scale $[x]$ to balance the gravity and pressure term in the momentum equation, as was done earlier, but this gives a length scale longer than typical bedform instabilities, and since our goal is to examine the latter we choose $[x]$ to be on the order of observed dune wavelengths. The scale for bedload flux $[q_b]$ is also assumed known once the scale for the velocity (and hence shear stress) has been chosen.

This results in the dimensionless equations

$$h = \eta - s, \tag{2.76}$$

$$\varepsilon\frac{\partial h}{\partial t} + \frac{\partial}{\partial x}(hu) = 0, \tag{2.77}$$

$$F^2\left(\varepsilon\frac{\partial u}{\partial t} + u\frac{\partial u}{\partial x}\right) = \delta\left(1 - \frac{u^2}{h}\right) - \frac{\partial \eta}{\partial x}, \tag{2.78}$$

$$\frac{\partial s}{\partial t} + \frac{\partial q}{\partial x} = 0, \tag{2.79}$$

where the parameters are

$$\varepsilon = \frac{[x]}{[u][t]}, \quad F = \frac{[u]}{\sqrt{g[h]}}, \quad \delta = \frac{S[x]}{[h]}, \tag{2.80}$$

and where the dimensionless bedload function can be taken to be a function of velocity, $q = q(u)$ (this is derived from the dimensional $q_b(\tau)$, but τ is directly related to u, and since u is a primary variable in our model it is easier to write it this way).

Here ε is the ratio of the advective timescale to the sediment transport timescale, which we expect to be small (note $\varepsilon = [q_b]/(1-n)Q$ so represents the ratio of sediment flux to water flux). In addition, we expect δ to be small, since the dune wavelengths are typically small compared to the natural length scale of the river (e.g. $S = 10^{-2}$, $[h] = 1$ m and $[x] = 10$ cm gives $\delta = 10^{-3}$). We can therefore approximate the problem by taking $\varepsilon \to 0$ and $\delta \to 0$.

The model simplifies to

$$hu = (\eta - s)u = 1, \tag{2.81}$$

$$F^2 u \frac{\partial u}{\partial x} = -\frac{\partial \eta}{\partial x}, \tag{2.82}$$

$$\frac{\partial s}{\partial t} + \frac{\partial q}{\partial x} = 0. \tag{2.83}$$

The second equation can be integrated to give

$$\tfrac{1}{2}F^2 u^2 + \eta = \tfrac{1}{2}F^2 + 1, \tag{2.84}$$

where we use uniform upstream conditions $u = 1$, $\eta = 1$ to evaluate the constant of integration. Alternatively, since $\eta = s + 1/u$, we can write this as a relationship between u and s,

$$s = \tfrac{1}{2}F^2(1 - u^2) + 1 - \frac{1}{u}. \tag{2.85}$$

There is a uniform steady state $s = 0$, $u = h = 1$, $q = q(1)$. We look for linear perturbations

$$u = 1 + U, \quad s = S, \tag{2.86}$$

and substituting into the equations (2.85) and (2.83) we have

$$S = (1 - F^2)U, \tag{2.87}$$

$$S_t + q'(1)U_x = 0. \tag{2.88}$$

Writing

$$S = e^{\sigma t + ikx}, \quad U = \hat{U}e^{\sigma t + ikx}, \tag{2.89}$$

we find

$$1 = (1 - F^2)\hat{U}, \tag{2.90}$$

and hence

$$\sigma = -\frac{ik}{1 - F^2}q'(1). \tag{2.91}$$

We see that there is no instability mechanism. Small perturbations neither grow not shrink, but are translated with speed $-\sigma_I/k = q'(1)/(1 - F^2)$, which is positive if $F < 1$ and negative if $F > 1$.

Since $\eta = s + 1/u$, the perturbation in surface elevation is

$$S - U = \frac{F^2}{F^2 - 1} e^{\sigma t + ikx}, \tag{2.92}$$

which is in phase with the bed elevation if $F > 1$ and out of phase if $F < 1$.

This model therefore correctly predicts the propagation direction of dunes and anti-dunes, as well as the relative phase of the bed and the stream surface, but it does not explain their growth from a uniform state.

Note that the Exner equation can be written in the form of a nonlinear wave equation for s,

$$\frac{\partial s}{\partial t} + q'(u)u'(s)\frac{\partial s}{\partial x} = 0, \tag{2.93}$$

where, from the relationship (2.85), we have

$$u'(s) = \frac{1}{s'(u)} = \frac{u^2}{1 - F^2 u^3}. \tag{2.94}$$

The wave speed can be both positive and negative depending on the value of F and on s, so the generic behaviour of many initial conditions is to form travelling waves that form shocks. In particular, dunes with $F < 1$ typically have downstream faces that steepen, whereas anti-dunes with $F > 1$ have upstream faces that steepen.

2.3.5 Suspended sediment

We now consider adding suspended sediment to the model. We make use of (2.66) and take dimensionless erosion rate $E = E(u)$, so the Exner equation and suspended sediment equation take the form

$$(1 - n)\frac{\partial s}{\partial t} + \frac{\partial q_b}{\partial x} = -v_s \left(E - \frac{c}{\rho_s} \right), \tag{2.95}$$

$$\frac{\partial}{\partial t}(hc) + \frac{\partial}{\partial x}(huc) = \rho_s v_s \left(E - \frac{c}{\rho_s} \right), \tag{2.96}$$

together with the St Venant equations in the form

$$\frac{\partial h}{\partial t} + \frac{\partial}{\partial x}(hu) = 0, \tag{2.97}$$

$$\frac{\partial u}{\partial t} + u\frac{\partial u}{\partial x} = g\left(S - \frac{\partial \eta}{\partial x} \right) - \frac{fu^2}{h}, \tag{2.98}$$

We non-dimensionalise the model, using scales

$$x = [x]\hat{x}, \quad t = [t]\hat{t}, \quad u = [u]\hat{u}, \quad s, h, \eta = [h]\left(\hat{s}, \hat{h}, \hat{\eta}\right), \quad c = [c]\hat{c}, \quad E = [E]\hat{E}, \quad q_b = [q_b]\hat{q}. \tag{2.99}$$

As before, the balance of terms in the momentum equation suggests that we choose scales so that

$$gS[h] = f[u]^2, \tag{2.100}$$

and we take the flux scale $Q = [h][u]$ as given, so choose scales

$$[h] = \left(\frac{fQ^2}{gS}\right)^{1/3}, \quad [u] = \left(\frac{gSQ}{f}\right)^{1/3}, \quad [t] = \frac{(1-n)[h]}{v_s[E]}, \quad [c] = \rho_s[E], \quad [x] = \frac{Q}{v_s}. \quad (2.101)$$

Note that, unlike for the bedload-only model, there is a natural length scale for deposition in this model, and we choose the length scale $[x]$ according to this. We also now choose the timescale associated with erosion, rather than with bedload transport, and will therefore introduce a parameter below to measure the size of the dimensionless bedload flux.

The dimensionless equations are

$$h = \eta - s, \quad (2.102)$$

$$\varepsilon\frac{\partial h}{\partial t} + \frac{\partial}{\partial x}(hu) = 0, \quad (2.103)$$

$$F^2\left(\varepsilon\frac{\partial u}{\partial t} + u\frac{\partial u}{\partial x}\right) = \delta\left(1 - \frac{u^2}{h}\right) - \frac{\partial \eta}{\partial x}, \quad (2.104)$$

$$\frac{\partial s}{\partial t} + \beta\frac{\partial q}{\partial x} = c - E, \quad (2.105)$$

$$\varepsilon\frac{\partial}{\partial t}(hc) + \frac{\partial}{\partial x}(huc) = E - c, \quad (2.106)$$

where the parameters are

$$\varepsilon = \frac{[x]}{[u][t]}, \quad F = \frac{[u]}{\sqrt{g[h]}}, \quad \delta = \frac{S[x]}{[h]}, \quad \beta = \frac{[q_b][t]}{[h][x]}. \quad (2.107)$$

Both $E = E(u)$ and $q = q(u)$ are taken to be dimensionless functions of velocity.

As in the previous section, we can reasonably expect to have $\varepsilon \ll 1$ and $\delta \ll 1$ (note that now $\varepsilon = [E]/(1-n)$ is the ratio of the advective timescale to the erosion timescale, and since $[E]$ dictates the suspended volume fraction, we expect this to be 10^{-2} or smaller; $\delta = S[u]/v_s$ can now be interpreted as the ratio of vertical velocity to settling velocity).

The model simplifies to

$$hu = (\eta - s)u = 1, \quad (2.108)$$

$$F^2 u\frac{\partial u}{\partial x} = -\frac{\partial \eta}{\partial x}, \quad (2.109)$$

$$\frac{\partial s}{\partial t} + \beta\frac{\partial q}{\partial x} = c - E = -\frac{\partial c}{\partial x}. \quad (2.110)$$

As earlier, the second equation can be integrated to give

$$\tfrac{1}{2}F^2u^2 + \eta = \tfrac{1}{2}F^2 + 1, \quad (2.111)$$

where we use uniform upstream conditions $u = 1$, $\eta = 1$ to evaluate the constant of integration.

There is a uniform steady state $s = 0$, $u = h = 1$, $c = E(1)$, $q = q(1)$. We look for linear perturbations

$$u = 1 + U, \quad c = E(1) + C, \quad s = S. \quad (2.112)$$

Substituting into the equations we have

$$S = (1 - F^2)U, \quad (2.113)$$

$$S_t + \beta q'(1) U_x = C - E'(1)U = -C_x. \tag{2.114}$$

Writing

$$S = e^{\sigma t + ikx}, \quad U = \hat{U} e^{\sigma t + ikx}, \quad C = \hat{C} e^{\sigma t + ikx}, \tag{2.115}$$

we find

$$1 = (1 - F^2)\hat{U}, \quad \hat{C} = \frac{E'(1)}{1 + ik}\hat{U}, \tag{2.116}$$

and hence

$$\sigma = \frac{E'(1)}{F^2 - 1}\frac{k^2}{1 + k^2} - \frac{ik}{1 - F^2}\left(\beta q'(1) + E'(1)\right). \tag{2.117}$$

On physical grounds we expect $E'(1) > 0$ and $q'(1) > 0$. We see that the growth rate σ_R is positive if $F > 1$ and negative if $F < 1$. The wave speed $-\sigma_I/k$ is positive if $F < 1$ and negative if $F > 1$.

This model therefore predicts the growth of upstream-propagating anti-dunes when $F > 1$. It correctly predict the direction of propagation of dunes for $F < 1$, but does not explain their growth. Note that the destabilisation for $F > 1$ comes entirely from the erosion term rather than the bed-load, consistent with the analysis in the previous section.

Note also that the growth rate is positive even for short wavelengths ($k \to \infty$). This is a sign of ill-posedness, since it suggests that very small scale perturbations in initial conditions would grow exponentially. Usually, this indicates that some other process that would regularise very small wavelength perturbations is missing from the model. In this case, we have neglected diffusion of the suspended sediment, and we have neglected the effect of gravity on the particles in the bed (which provides a modification to the bedload flux depending on the perturbed bed slope).

2.3.6 Eddy viscosity model

The above calculations have shown that it is not possible to predict the formation of dunes using the St Venant-type, depth-integrated, stream model. However, it *is* possible to do so if we use a description of the water flow that accounts for vertical variations in velocity. Models of this form include potential flow models (for inviscid flow), or eddy viscosity models for turbulent flow. We do not go into these here, but report that the results of a more detailed calculation (based on the solution of the Orr-Sommerfeld equation), lead to the following expression for the basal shear stress,

$$\tau = \frac{f\rho_w \overline{u}^2}{\overline{h}}\left[\overline{h} - s + \int_{-\infty}^{\infty} K(x - \xi)\frac{\partial s}{\partial \xi}(\xi)\, \mathrm{d}\xi\right], \tag{2.118}$$

with $K(x) = \mu x^{-1/3}\mathcal{H}(x)$, $\overline{u}$ the mean stream speed, and $\overline{h}$ the mean depth. This allows τ to depend on the bed slope $\partial s/\partial x$ upstream.

It can be shown (exercise) that a model including this modified relationship for the shear stress can predict the formation of dunes for $F < 1$, as observed.

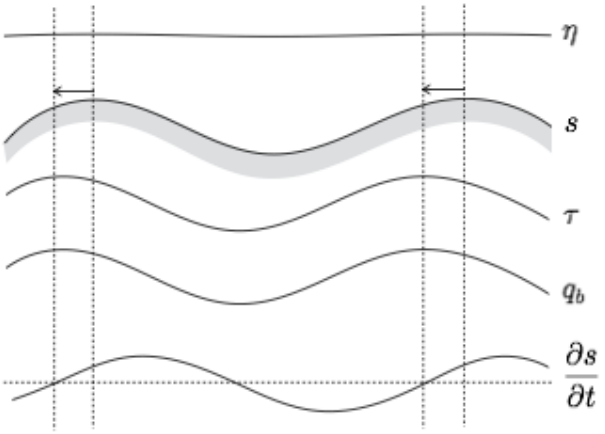

Figure 2.10: Instability mechanism for dune formation; the maximum shear stress and hence bedload transport occurs slightly upstream of the maximum bed height.

2.3.7 Instability mechanism

The essential ingredient for the formation of dunes that appears to be lacking from the depth-integrated theories is that there should be a lag between local maxima in the bed and the maximum shear stress exerted on the bed.

In our models, the maximum shear stress occurs always at the same location as the maximum in the bed height, because the velocity there is largest (this is easiest to see from looking at the perturbations, where U and S are always proportional for $F < 1$). But for the system to be unstable to the formation of dunes, the maximum shear stress, and therefore the maximum bedload flux or erosion rate, must be slightly upstream of the maxima in the bed height. In that case the sediment load is largest upstream of each bump and sediment is therefore being deposited back onto the bed at the top of the bump, causing it to grow. (In the absence of erosion and deposition the rate of change of bed height is proportional to $-\partial q_b/\partial x$, and so the region ahead of the maxima of q_b will see grow taller and the region behind will fall; this also explains why the dunes move forwards over time).

A crude way to include this lag, that does exist in the mode detailed eddy-viscosity model, is to suppose that the shear stress is a function of the the velocity a short distance further downstream, so $\tau(x,t) = f\rho_w(u(x+\delta,t))^2$, where δ represents the lag. Combining with the Exner equation and assuming that the water surface remains flat $\eta = 1$ (as follows from the momentum equation for small F and over short length scales), we have the dimensionless model

$$\frac{\partial s}{\partial t} + q'(\tau)\frac{\partial \tau}{\partial x} = 0, \qquad \tau(x,t) = \frac{1}{(1-s(x+\delta,t))^2}. \tag{2.119}$$

The steady state $s = 0$ can be perturbed to give perturbation $S(x,t)$ satisfying

$$\frac{\partial S}{\partial t}(x,t) + 2q'(1)\frac{\partial S}{\partial x}(x+\delta,t) = 0. \tag{2.120}$$

Solutions of the form $S = e^{\sigma t + ikx}$ require

$$\sigma = -2ikq'(1)e^{ik\delta}, \tag{2.121}$$

for which the growth rate is $\sigma_R = 2q'(1)k\sin k\delta > 0$ and the wave speed is $-\sigma_I/k = 2q'(1)\cos k\delta > 0$. This model therefore predicts the formation of dunes (note that we should

restrict attention to values of k for which $k\delta \ll 1$, since the lag we artificially introduced should not be longer than the wavelength of the perturbations under consideration).

3 Glaciers

Glaciers build up over time through the accumulation of snow, which compacts under its weight to form ice. With sufficient weight the ice can flow, by viscous creep or by slipping over the underlying rock. The accumulation generally occurs at high elevations, where the annual balance between snowfall and melting is positive. At lower elevations, melting outpaces snowfall, and a glacier would not be able to form there, were it not for the flow of ice from higher elevations. Of course, latitude is also a big factor in determining where a glacier can form, because air temperatures are considerably colder at higher latitudes so there is less melting there.

Glaciers therefore act in a similar way to rivers, transporting ice from higher elevations to lower ones. In some cases, as for most rivers, the glaciers reach all the way to the ocean and discharge the ice as icebergs into the ocean (sometimes the ice flows into a floating *ice shelf* before breaking off). In other cases the glacier loses all its mass to melting before it reaches the ocean (the analogue for a river would be in a hot environment where evaporation or seepage into the ground (e.g. limestone) causes the river to dry up before it reaches the ocean).

An *ice sheet* is essentially the same as a glacier, but larger. The distinction is blurry, but a glacier usually has a well defined flow direction, whereas an ice sheet flows in all directions (the canonical ice sheet is radially symmetric, whereas a glacier is essentially one-dimensional). An *ice cap* is often used to mean a small ice sheet. There are currently two ice sheets on Earth; one in Antarctica and one in Greenland. During the glacial periods of the last two millennia there were two other large ones; the Laurentide ice sheet (covering much of North America), and the Fennoscandian ice sheet (covering Scandinative, the North Sea, and the British Isles), as well as smaller ice caps in Arctic Russia and the Canadian Archipelago.

The typical speeds of a glacier are around 100 m y^{-1}, but they can in places move at speeds greater than 1 km y^{-1}. This depends upon the temperature of the ice, which controls its effective viscosity (similar to honey), and on the slipperiness of the substrate over which it is moving (the substrate is sometimes rigid bedrock and sometimes water-saturated sediments which can themselves deform). Mountain glaciers (in the Alps, Himalaya, etc.) are typically several hundred meters deep, tens of kilometers long, and have surface slopes on the order of 0.1. The Antarctic and Greenland ice sheets on the other hand are around 3 km deep and 3000 km wide.

In this chapter we describe the equations that govern the flow and melting of glaciers and ice sheets. We will consider steady states, look at how perturbations to the steady states evolve, and how the glaciers can be expected to respond to climate change. We also discuss explanations for some of the more interesting behaviour that is observed: glacier surges, and outburst floods.

3.1 Shallow ice approximation

The starting point for modelling ice flow is the constitutive law, or flow law, that describes viscous deformation. This will be combined with statements of mass and momentum conservation (force balance) to arrive at an evolution equation for the thickness of the glacier. We use an approximate form of the momentum equation appropriate for thin layers of viscous

fluid; the necessary approximations can be introduced immediately in the model derivation, or can be justified more systematically using lubrication theory.

3.1.1 Glen's flow law

Glacial ice is a polycrystalline material; it is composed of many crystals that deform under stress by a combination of dislocation creep (the motion of dislocations through the crystal structure) and diffusion creep (the diffusion of molecules along the crystal interfaces). The deformation is usually described by Glen's flow law,

$$\dot{\varepsilon}_{ij} = A\tau^{n-1}\tau_{ij}, \tag{3.1}$$

where $\tau = \sqrt{\frac{1}{2}\tau_{ij}\tau_{ij}}$ is the second invariant of the deviatoric stress tensor τ_{ij} (the summation convention is used here), and where $n \approx 3$, and $A = A(T)$ is a temperature-dependent rate factor. Here $\dot{\varepsilon}_{ij}$ is the strain rate tensor, defined in terms of the velocity $\mathbf{u} = u_i$ by

$$\dot{\varepsilon}_{ij} = \frac{1}{2}\left(\frac{\partial u_i}{\partial x_j} + \frac{\partial u_j}{\partial x_i}\right), \tag{3.2}$$

and the deviatoric stress tensor is related to the full (Cauchy) stress tensor σ_{ij} by

$$\sigma_{ij} = -p\delta_{ij} + \tau_{ij}, \qquad p = -\tfrac{1}{3}\sigma_{kk}. \tag{3.3}$$

The flow law can be written in the more standard framework of viscous fluid mechanics as

$$\tau_{ij} = 2\eta\dot{\varepsilon}_{ij}, \tag{3.4}$$

where $\eta = 1/2A\tau^{n-1}$ is the *effective* viscosity. For a Newtonian fluid ($n = 1$), the viscosity is constant, but for $n \neq 1$, it depends on the stress. Fluids with $n > 1$, as is the case for ice, are referred to as shear thinning fluids, since the viscosity decreases with increasing stress.

For ice in a glacier, which has a small aspect ratio ($z \ll x$), the dominant component of the deviatoric stress tensor is usually $\tau_{xz} \approx \tau$, and the dominant component of the strain rate tensor is $\dot{\varepsilon}_{xz}$, so the flow law can be written approximately as

$$\frac{\partial u}{\partial z} = 2A\tau^n. \tag{3.5}$$

(Here we have assumed that $\tau_{xz} \approx \tau$ is positive; more generally, the right hand side is $2A|\tau|^{n-1}\tau$.)

The flow law coefficient A depends strongly on temperature, but we will treat it as constant for the rest of this section. This corresponds either to ignoring the temperature dependence, or to assuming that the ice is isothermal.

3.1.2 Mass conservation

We consider a two-dimensional glacier and use coordinates (x, z) for the horizontal and vertical directions. The bed is denoted $z = b(x)$ and the surface is denoted $z = s(x, t)$. We assume for simplicity that the surface elevation is monotonically decreasing, $\partial s/\partial x < 0$.

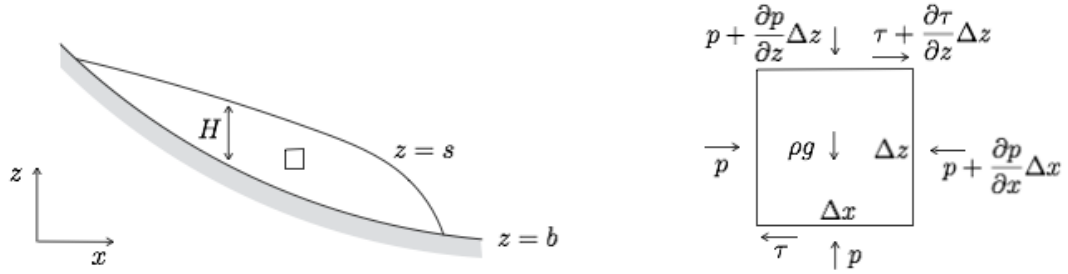

Figure 3.1: Glacier geometry and approximate force balance on arbitrarily small volumes of the ice.

The mass conservation equation can be derived, as it was for a river, by considering the mass of ice in a section between points x_1 and x_2. This results in

$$\frac{\partial H}{\partial t} + \frac{\partial q}{\partial x} = a, \tag{3.6}$$

where $H(x,t) = s - b$ is the ice thickness, $q(x,t)$ is the flux, and $a(x,t)$ is the net accumulation, being the difference between snowfall and melt.

Ice flux is given in terms of the velocity profile by

$$q(x,t) = \int_b^s u(x,z,t)\ \mathrm{d}z. \tag{3.7}$$

The velocity profile is derived from consideration of force balance.

3.1.3 Force balance

The importance of acceleration in the flow of a glacier is measured by the Reynolds number,

$$Re = \frac{\rho[u][h]}{[\eta]}, \tag{3.8}$$

where $\rho \approx 916$ kg m^{-3} is the density and $[u]$, $[h]$ and $[\eta]$ are typical values of the velocity, depth and viscosity. Taking $[u] = 30$ m y^{-1} $\approx \times 10^{-6}$ m s^{-1}, $[h] = 100$ m, and $[\eta] = 10^{12}$ Pa s, gives $Re \approx 10^{-13}$. We see that the Reynolds number is very small, and the acceleration terms are therefore negligible.

Based on the fact that the aspect ratio is small, we assume that we can also ignore deviatoric longitudinal stresses (compression and extension) and vertical shear stress.

We can then derive the equations by considering the forces acting on a small rectangle of ice, Δx by Δz. The relevant terms are the pressure p, viscous shear stress $\tau = \tau_{xz}$, and gravity g. Balancing the forces in the x and z directions respectively gives

$$0 = -\frac{\partial p}{\partial x} + \frac{\partial \tau}{\partial z}, \tag{3.9}$$

$$0 = -\frac{\partial p}{\partial z} - \rho g. \tag{3.10}$$

The surface of the glacier $z = s(x,t)$ is assumed stress free, so the boundary conditions that go with these equations are

$$p = \tau = 0 \quad \text{at} \quad z = s(x,t). \tag{3.11}$$

The equations can be integrated immediately to give

$$p = \rho g(s-z), \qquad \tau = -\rho g \frac{\partial s}{\partial x}(s-z). \tag{3.12}$$

We can then substitute the shear stress into the approximate flow law (3.5) and integrate using no-slip condition $u = 0$ at the bed $z = b$, to obtain

$$u = \frac{2A(\rho g)^n}{n+1}\left(-\frac{\partial s}{\partial x}\right)^n \left(H^{n+1} - (s-z)^{n+1}\right). \tag{3.13}$$

Substituting this into (3.7) gives

$$q = \frac{2A(\rho g)^n}{n+2}\left(-\frac{\partial s}{\partial x}\right)^n H^{n+2}. \tag{3.14}$$

Had we not assumed $\partial s/\partial x < 0$, the more general of this relationship that allows flow in both directions is

$$q = -\frac{2A(\rho g)^n}{n+2}\left|\frac{\partial s}{\partial x}\right|^{n-1}\frac{\partial s}{\partial x}H^{n+2}. \tag{3.15}$$

3.1.4 *Lubrication theory

A more systematic method of deriving the equations for glacier flow is to start from the Stokes equations (in two dimensions),

$$\frac{\partial u}{\partial x} + \frac{\partial w}{\partial z} = 0, \tag{3.16}$$

$$0 = -\frac{\partial p}{\partial x} + \frac{\partial \tau_{xx}}{\partial x} + \frac{\partial \tau_{xz}}{\partial z}, \tag{3.17}$$

$$0 = -\frac{\partial p}{\partial z} + \frac{\partial \tau_{xz}}{\partial x} + \frac{\partial \tau_{zz}}{\partial z} - \rho g, \tag{3.18}$$

together with the full flow law (3.2). The boundary conditions that go with this full problem are the no slip and no penetration conditions at the bed,

$$u = w = 0 \quad \text{at} \quad z = b(x,t), \tag{3.19}$$

the kinematic condition at the surface

$$\frac{\partial s}{\partial t} + u\frac{\partial s}{\partial x} = w + a \quad \text{at} \quad z = s(x,t), \tag{3.20}$$

and the stress-free conditions at the surface

$$-(-p + \tau_{xx})\frac{\partial s}{\partial x} + \tau_{xz} = 0, \tag{3.21}$$

$$-\tau_{xz}\frac{\partial s}{\partial x} + (-p + \tau_{zz}) = 0. \tag{3.22}$$

The neglect of the acceleration terms from the left hand side is justified by the smallness of the Reynolds number, discussed above. If we now non-dimensionalise, with $x \sim [x]$ and $z \sim [H]$, and define the aspect ratio

$$\varepsilon = \frac{[H]}{[x]}, \tag{3.23}$$

it is appropriate to scale the other terms as

$$[p] = \rho g[H], \quad [\tau_{xz}] = [\tau] = \varepsilon\rho g[H], \quad [\tau_{xx}] = [\tau_{zz}] = \varepsilon[\tau], \quad [u] = A[\tau]^n[H], \quad [w] = \varepsilon[u], \tag{3.24}$$

The dimensionless force-balance equations become

$$0 = -\frac{\partial p}{\partial x} + \varepsilon^2\frac{\partial \tau_{xx}}{\partial x} + \frac{\partial \tau_{xz}}{\partial z}, \tag{3.25}$$

$$0 = -\frac{\partial p}{\partial z} + \varepsilon^2\frac{\partial \tau_{xz}}{\partial x} + \varepsilon^2\frac{\partial \tau_{zz}}{\partial z} - 1, \tag{3.26}$$

and the boundary conditions are

$$-(-p + \frac{\varepsilon^2}{\mu}\tau_{xx})\frac{\partial s}{\partial x} + \tau_{xz} = 0, \tag{3.27}$$

$$-\varepsilon^2\tau_{xz}\frac{\partial s}{\partial x} + (-p + \varepsilon^2\tau_{zz}) = 0. \tag{3.28}$$

The only relevant component of the flow law that is needed for the leading order problem is the xz component,

$$\frac{1}{2}\left(\frac{\partial u}{\partial z} + \varepsilon^2\frac{\partial w}{\partial x}\right) = \tau^n\tau_{xz}, \tag{3.29}$$

where the second invariant of the stress tensor is

$$\tau^2 = \tau_{xz}^2 + \varepsilon^2\tau_{xx}^2. \tag{3.30}$$

If we now take the limit $\varepsilon \to 0$, the equations become the same as those used earlier in (3.9) and (3.10) (though already non-dimensionalised),

$$0 = -\frac{\partial p}{\partial x} + \frac{\partial \tau}{\partial z}, \tag{3.31}$$

$$0 = -\frac{\partial p}{\partial z} - 1, \tag{3.32}$$

together with the flow law as in (3.5),

$$\frac{\partial u}{\partial z} = 2\tau^n. \tag{3.33}$$

We can also integrate the pointwise conservation of mass equation (3.16) with the boundary conditions (3.19) and (3.20) to obtain the depth-integrated conservation equation,

$$\int_b^s \frac{\partial u}{\partial x}\,\mathrm{d}z = -\int_b^s \frac{\partial w}{\partial z}\,\mathrm{d}z, \tag{3.34}$$

$$= -[w]_b^s, \tag{3.35}$$

$$\frac{\partial}{\partial x}\left(\int_b^s u\,\mathrm{d}z\right) - u\big|_s\frac{\partial s}{\partial x} + u\big|_b\frac{\partial b}{\partial x} = -\frac{\partial s}{\partial t} - u\big|_s\frac{\partial s}{\partial x} + a, \tag{3.36}$$

$$\frac{\partial}{\partial x}\left(\int_b^s u\,\mathrm{d}z\right) = -\frac{\partial H}{\partial t} + a, \tag{3.37}$$

which is the same as (3.6),

$$\frac{\partial H}{\partial t} + \frac{\partial q}{\partial x} = a. \tag{3.38}$$

3.2 Glaciers

To model a mountain glacier, we take the bed as being an approximately linear slope, with

$$\frac{\partial b}{\partial x} = -\tan\theta. \tag{3.39}$$

Assuming $\partial H/\partial x < \tan\theta$, so that the ice always flows in the positive x direction, the expression for the ice flux (3.14) then becomes

$$q = \frac{2A}{n+2}(\rho g)^n \left(\tan\theta - \frac{\partial H}{\partial x}\right)^n H^{n+2}, \tag{3.40}$$

which we combine with the mass equation

$$\frac{\partial H}{\partial t} + \frac{\partial q}{\partial x} = a. \tag{3.41}$$

3.2.1 Non-dimensionalisation

We non-dimensionalise by writing

$$x = [x]\hat{x}, \qquad t = [t]\hat{t}, \qquad H = [H]\hat{H}, \qquad q = [q]\hat{q}, \qquad a = [a]\hat{a}. \tag{3.42}$$

We assume that the accumulation scale $[a]$ and the length scale $[x]$ are known (from climatic conditions and from the topography of the mountain range). We are then free to choose

$$[q] = [a][x], \qquad [H] = \left(\frac{[q]}{2A(\rho g\tan\theta)^n}\right)^{1/(n+2)}, \qquad [t] = \frac{[H][x]}{[q]}, \tag{3.43}$$

and define

$$\mu = \frac{[H]}{[x]}\cot\theta. \tag{3.44}$$

The dimensionless mass conservation equation then becomes (dropping hats),

$$\frac{\partial H}{\partial t} + \frac{\partial}{\partial x}\left[\left(1 - \mu\frac{\partial H}{\partial x}\right)^n \frac{H^{n+2}}{n+2}\right] = a. \tag{3.45}$$

Typical values are $n = 3$, $A = 10^{-24}$ Pa^{-3} s^{-1}, $\rho = 916$ kg m^{-3}, $g = 9.8$ m s^{-2}, $\tan\theta = 0.1$, $[a] = 1$ m y^{-1}, and $[x] = 10^4$ m, from which $[q] = 3\times10^{-4}$ m^2 s^{-1}, $[H] \approx 200$ m, $[t] = 200$ y, and $\mu \approx 0.2$. Note that $[t] = [x]/[u]$ is the natural advective timescale of the glacier, giving the timescale over which ice moves along its length.

3.2.2 Steady states and surface waves

The governing equation (3.45) is a nonlinear diffusion equation for H, given a prescribed source term a, which we can assume is determined by the local climate. The equation is very similar to the equation that governs the flow of a drop down an inclined plane (indeed, it *is* the same if the drop is that of a shear thinning fluid).

The typical values of μ are relatively small and it is reasonable to neglect the diffusion term, to arrive at a hyperbolic equation (analogous to that which describes the depth of a river),

$$\frac{\partial H}{\partial t} + H^{n+1}\frac{\partial H}{\partial x} = a. \tag{3.46}$$

This is a nonlinear wave equation, with solutions that propagate as waves and, generically, form shocks. Such shocks would in reality be smoothed out by the presence of the diffusive term. If $x = 0$ is the head of the glacier, the appropriate boundary condition is $H = 0$ there, and a similar condition $H = 0$ at $x = x_m$ determines the location of the glacier terminus x_m (this is a form of 'free boundary' - determining the location of the terminus is part of the problem, and this explains why we can effectively have two boundary conditions on a first order equation).

For steady accumulation $a(x)$, the terminus position x_m is given by

$$0 = \int_0^{x_m} a(x)\ \mathrm{d}x. \tag{3.47}$$

The steady state ice depth is given by

$$H_0(x) = \left[(n+2)\int_0^x a(x')\ \mathrm{d}x'\right]^{1/(n+2)}. \tag{3.48}$$

For example, suppose $a = 1 - x$ (for a linearly sloping valley, this reflects the decrease in air temperature, and hence melt rate, with elevation). In this case $q = x - \frac{1}{2}x^2$, $x_m = 2$, and the depth is

$$H_0(x) = \left[(n+2)(x - \tfrac{1}{2}x^2)\right]^{1/(n+2)}. \tag{3.49}$$

We can also consider how perturbations to the steady state propagate. Such perturbations may be caused by a particularly large accumulation event such as an avalanche from the valley sidewalls, or they may be forced by the seasonal cycle of accumulation considered below.

We first consider exact solutions for an initial perturbation, and then consider linearised versions of the equation for small perturbations.

The exact problem (3.46) for $a(x)$ with $H = H_{in}(x)$ at $t = 0$ can be solved using the method of characteristics,

$$\dot{x} = H^{n+1}, \qquad \dot{H} = a, \tag{3.50}$$

with initial data

$$x = x_0 \quad H = H_{in}(x_0), \qquad \text{at} \quad t = 0, \tag{3.51}$$

Dividing the characteristic equations by each other and integrating, recalling the definition of $H_0(x)$ in (3.48), we obtain

$$H(x,t)^{n+2} = H_0(x)^{n+2} - H_0(x_0)^{n+2} + H_{in}(x_0)^{n+2}, \tag{3.52}$$

where $x_0(x,t)$ is defined implicitly by

$$t = \int_{x_0}^{x} \frac{\mathrm{d}x'}{\left[H_0(x')^{n+2} - H_0(x_0)^{n+2} + H_{in}(x_0)^{n+2}\right]^{\frac{n+1}{n+2}}}. \tag{3.53}$$

This provides the exact solution for a given initial condition, but it is not particularly illuminating. More progress can be made if we (reasonably) assume that the initial condition is close to the steady state.

Suppose $H(x,t) = H_0(x) + H_1(x,t)$, where $H_1 \ll H_0$. We can then linearise equation (3.46), giving

$$\frac{\partial H_1}{\partial t} + \frac{\partial}{\partial x}\left[H_0^{n+1} H_1\right] = 0. \tag{3.54}$$

This can be solved by multiplying by $H_0(x)^{n+1}$ to give

$$\frac{\partial}{\partial t}\left[H_0^{n+1} H_1\right] + H_0^{n+1}\frac{\partial}{\partial x}\left[H_0^{n+1} H_1\right] = 0, \tag{3.55}$$

and then defining a distorted space variable,

$$\xi = \int_0^x \frac{\mathrm{d}x'}{H_0(x')^{n+1}}, \tag{3.56}$$

so that

$$\frac{\partial}{\partial t}\left[H_0^{n+1} H_1\right] + \frac{\partial}{\partial \xi}\left[H_0^{n+1} H_1\right] = 0. \tag{3.57}$$

This has the travelling wave solution (using the method of characteristics, or just by inspection) $H_0^{n+1} H_1 = \phi(\xi - t)$ for arbitrary function ϕ determined from the initial condition. This solution takes the form of a travelling wave, moving with constant speed in the distorted space coordinate. The perturbation to the ice depth is therefore

$$H_1(x,t) = \frac{\phi(\xi - t)}{H_0(x)^{n+1}}, \qquad \xi = \int_0^x \frac{\mathrm{d}x'}{H_0(x')^{n+1}}. \tag{3.58}$$

The speed of the perturbations is

$$\frac{\partial x}{\partial \xi} = H_0(x)^{n+1}, \tag{3.59}$$

and is therefore $n+1$ times the surface ice speed (which, from (3.13) after non-dimensionalising, is $H_0^{n+1}/(n+1)$). So the perturbation in surface height moves faster than the ice itself.

There is a problem with this solution, however, because the amplitude of the perturbation blows up at the terminus where H_0 goes to zero. This invalidates the linearisation, since H_1 was assumed small compared to H_0 in deriving (3.54). This issue is related to the fact that the terminus x_m is really a free boundary, the position of which should be perturbed at the same time as the ice depth. Depth perturbations go together with perturbations of the fluid front. A number of methods can be used to study the movement of the front, notably the method of strained coordinates; but we do not go into that here.

An alternative method of linearising the equation is to approximate the characteristic equations

$$\dot{x} = H^{n+1} \approx H_0^{n+1}, \qquad \dot{H} = a \implies \dot{H}_0 = a, \quad \dot{H}_1 = 0. \tag{3.60}$$

This is not quite the same linearisation, as it corresponds to solving the perturbation equation

$$\frac{\partial H_1}{\partial t} + H_0^{n+1}\frac{\partial H_1}{\partial x} = 0, \tag{3.61}$$

which can be solved with the same change of variables as above to give

$$H_1(x,t) = \phi(\xi - t) \qquad \xi = \int_0^x \frac{\mathrm{d}x'}{H_0(x')^{n+1}}, \tag{3.62}$$

where $\phi(\xi - t)$ is determined from the initial condition. This perturbation does not blow up at the terminus. The missing term in this linearisation compared to the earlier one is $(n+1)H_0^n H_1 \partial H_0/\partial x$, and the neglect of this term can be justified if $\partial H_0/\partial x$ is small on the length scale of the perturbation (*i.e.* if $H_0 \partial H_1/\partial x > H_1 \partial H_0/\partial x$).

3.2.3 Seasonal fluctuations

If we resolve annual timescales, the accumulation fluctuates over most of the glacier between positive (during winter) and negative (during summer). We can analyse the seasonal oscillations of a glacier governed by

$$\frac{\partial H}{\partial t} + H^{n+1}\frac{\partial H}{\partial x} = a(x,t), \tag{3.63}$$

by defining the annual average accumulation and ice thickness

$$\overline{a}(x) = \frac{1}{t_y}\int_0^{t_y} a(x,t)\ \mathrm{d}t, \qquad \overline{H}(x) = \frac{1}{t_y}\int_0^{t_y} H(x,t)\ \mathrm{d}t. \tag{3.64}$$

Here t_y is the (dimensionless) length of a year. We also write $a(x,t) = \overline{a}(x) + a_1(x,t)$, $H(x,t) = \overline{H}(x) + H_1(x,t)$ and suppose $H_1 \ll \overline{H}$, so that we can linearise the equation around $\overline{H}$ (using the second of the two linearisation methods above),

$$\frac{\partial H_1}{\partial t} + \overline{H}^{n+1}\frac{\partial \overline{H}}{\partial x} + \overline{H}^{n+1}\frac{\partial H_1}{\partial x} = \overline{a} + a_1. \tag{3.65}$$

Then averaging the equation in time shows that the average state is given by

$$\frac{\partial}{\partial x}\left[\frac{\overline{H}^{n+2}}{n+2}\right] = \overline{a}, \tag{3.66}$$

and the perturbation is governed by

$$\frac{\partial H_1}{\partial t} + \overline{H}^{n+1}\frac{\partial H_1}{\partial x} = a_1. \tag{3.67}$$

For example, if $a_1(x,t) = \cos\omega t$, where $\omega = 2\pi/t_y$, and $H = 0$ at $x = 0$, then

$$H_1 = \frac{2}{\omega}\cos\tfrac{1}{2}\omega(\xi - 2t)\sin\tfrac{1}{2}\omega\xi, \qquad \xi = \int_0^x \frac{\mathrm{d}x'}{\overline{H}(x')^{n+1}}. \tag{3.68}$$

The timescale used to scale the equation was the natural advective timescale of the glacier $[t] = [h]/[u]$, and is much larger than a year, so the dimensionless frequency ω is large. Thus the perturbation H_1 is small, justifying the linearisation. We see that the annual accumulation signal gives rise to small surface waves that propagate down glacier.

3.3 Glacier sliding

In the previous section we assumed that the ice had a no-slip condition at the bed, $u = 0$ at $z = b$. This is appropriate if the ice is frozen to the bed, but is usually not correct if the ice at the bed is at the melting point. In that case there is a thin film of water between the ice and the bedrock, which lubricates the interface and allows slip. Perhaps surprisingly, such conditions of melting ice at the bed are very common, because of geothermal and frictional heating, and because the thick layer of ice insulates the bed from the cold air temperatures.

The slip is parameterised mathematically using a boundary condition of the form

$$\tau_b = f(u_b), \tag{3.69}$$

where $\tau_b = \tau|_{z=b}$ is the basal shear stress, and $u_b = u|_{z=b}$ is the sliding speed. This is referred to as the friction law or sliding law. Note that the basal shear stress is known from (3.12) and is approximately $\rho g H \tan\theta$ for a glacier.

A common version of this sliding law is

$$u_b = C|\tau_b|^{m-1}\tau_b, \tag{3.70}$$

where C and m are constants, which parameterise the detailed small-scale physics that allows for sliding. This is referred to as a Weertman sliding law.

On hard bedrock, sliding is believed to result from lubricated viscous flow around small-scale bedrock obstacles, and by a process called regelation. We discuss both of these below. When a glacier moves over sediments, sliding can result from the same processes, but may additionally be due to the deformation (flow) of the sediments themselves. When water-saturated, the sediments can be considerably less stiff than the ice, and they similarly deform in a viscous manner, driven by the weight of the ice.

Using the sliding law (3.70) as the boundary condition when determining the velocity profile results in an additional term,

$$u_b H = C(\rho g)^m \left(-\frac{\partial s}{\partial x}\right)^m H^{m+1}, \tag{3.71}$$

in the vertically-integrated ice flux (3.14). Following the same non-dimensionalisation as above, the mass conservation equation for the glacier (3.45) then becomes

$$\frac{\partial H}{\partial t} + \frac{\partial}{\partial x}\left[\gamma\left(1-\mu\frac{\partial H}{\partial x}\right)^m \frac{H^{m+1}}{m+1} + \left(1-\mu\frac{\partial H}{\partial x}\right)^n \frac{H^{n+2}}{n+2}\right] = a, \tag{3.72}$$

(assuming $\partial H/\partial x < 1/\mu$), where the dimensionless sliding coefficient is defined as

$$\gamma = \frac{(m+1)C}{2A}(\rho g \tan\theta)^{m-n}[H]^{m-n-1}. \tag{3.73}$$

Typical values are $m = 3$ and $C = 10^{-22}$ m s^{-1} Pa^{-3}, and using other values defined previously, this gives $\gamma \approx 10$. However, estimates for C are highly variable (it is not expected to take the same values everywhere), and a large range of values of γ are possible. Small γ corresponds to sliding having only a small influence on glacier flow; large γ corresponds to sliding dominating the flow (this is sometimes referred to as *plug* flow), and it may be appropriate to re-scale the equation in this case so that the sliding term balances the accumulation and time-derivative.

In the following sections we discuss the physical basis for adopting a sliding law of the form (3.70), and the additional role that subglacial water may play.

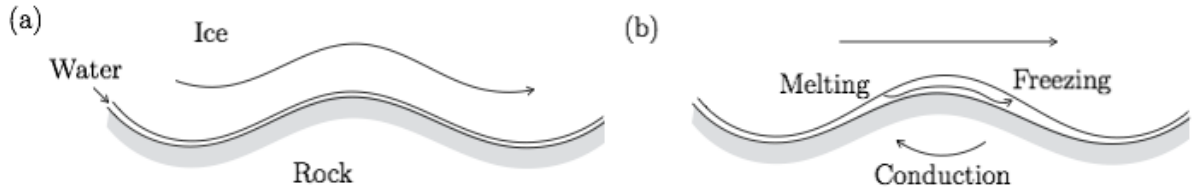

Figure 3.2: Sliding due to lubrication by a thin water film by (a) viscous flow, and (b) regelation.

3.3.1 Viscous sliding

The presence of a thin film of water between ice and the underlying substrate means that on a micro scale it is appropriate to apply a zero shear stress condition on the ice flow (compared to the ice, the water is essentially inviscid, so supports negligible shear stress). If the bed were perfectly flat, this would allow very rapid sliding, but this is never likely to be the case in reality. There are small (mm to m scale) bumps over which the ice must deform. Such roughness provides a resistance that supports the large scale shear stress τ_b (which is known from (3.12)).

Since the microscopic shear stress is zero, the resistance comes from normal stress differences between the upstream and downstream faces of obstacles in the bed. These can be crudely estimated on dimensional grounds from the Glen's flow law: if the sliding velocity is u_b, the strain rates associated with flowing over an obstacle of size a are of order u_b/a, and this gives rise to stress differences of order $(u_b/aA)^{1/n}$. If such obstacles occupy a fraction ν^2 of the bed (by area), this suggests that the flow over such obstacles can be parameterised by a sliding law of the form

$$\tau_b = \nu^2 (aA)^{-1/n} u_b^{1/n}. \tag{3.74}$$

A more satisfactory theoretical derivation of the sliding law can be performed if the ice is treated as Newtonian. In that case, assuming small amplitude roughness of the bed, a linearised model of the viscous fluid flow can be solved (using Fourier transforms), to find

$$\tau_b = \frac{\eta u_b}{\pi} \int_0^\infty \hat{B}(k) k^3 \, \mathrm{d}k, \tag{3.75}$$

where the integral is taken over all waveumbers, and $\hat{B}(k)$ is the Fourier transform of the micro-scale bed profile $Z = B(X)$. This makes clear that the basal stress depends on many scales of bed roughness.

3.3.2 *Regelation

A second process occurs at the same time as the viscous flow described above, and is more efficient at allowing ice to move past the smallest obstacles (note that the resistance goes to infinity as the obstacle size a goes to zero in the above expressions). This process is referred to as regelation. It relies upon the pressure-dependence of the melting point, which means that the temperature at the ice base (which is constrained to the melting point) is slightly

lower on the upstream faces of obstacles than on the downstream faces (due to the normal stress difference alluded to above). This results in melting of the ice on the upstream faces and freezing on the downstream faces. The flow of liquid water through the thin lubricating film, from locations of melting to freezing, effectively allows the ice to move 'through' the obstacles.

The rate at which this process allows the ice (and water) to move is controlled by the rate of melting and freezing. Since the phase changes consume and release energy, this rate is controlled by how quickly the energy released by freezing can conduct back through the obstacle to enable melting; this depends on the conductivity of the obstacle, and will be most efficient for small obstacles.

We can again crudely estimate the sliding rate due to this process by balancing the conductive heat flux through a bump, $k_b \Delta T/a$, with the latent heat required to melt the ice $\rho L u_b$. The temperature difference is due to the stress difference, τ_b/ν^2 if the obstacles occupy a fraction ν^2 of the bed, and the Clapeyron slope $C = -dT_m/dp$ (the gradient of the melting temperature with pressure), giving $\Delta T = C\tau_b/\nu^2$. The energy balance therefore gives a sliding law of the form

$$\tau_b = \nu^2 \frac{\rho L a}{k_b C} u_b. \tag{3.76}$$

3.3.3 *Weertman sliding

Writing the result for the two mechanisms (viscous flow and regelation) in the form $\tau_b = \nu^2 R_v a^{-1/n} u_b^{1/n}$ and $\tau_b = \nu^2 R_r a u_b$, we can combine them by taking the minimum,

$$\tau_b = \nu^2 \min\left(R_v a^{-1/n} u_b^{1/n}, R_r a u_b\right). \tag{3.77}$$

Since there are in reality a whole range of obstacle sizes, and the two mechanisms are more efficient at transporting ice past small and large obstacles respectively, there is a controlling obstacle size that provides the dominant resistance. This is given by $a = (R_v/R_r)^{n/(n+1)} u_b^{-(n-1)/(n+1)}$, and leads to the combined sliding law

$$\tau_b = \nu^2 R u_b^{2/(n+1)}, \tag{3.78}$$

where $R = (R_r R_v^n)^{1/(n+1)} = (\rho L/k_b C A)^{1/(n+1)}$. This is the same as (3.70), with $m = (n+1)/2$.

A modification of the linear theory described earlier for viscous sliding can be used to derive a law of this type more systematically. Assuming the ice to be Newtonian, and assuming small amplitude roughness we can solve for the viscous deformation of ice over the linearised bed, and for the conduction of heat through the rock beneath, together with boundary conditions on the interface itself that account for the latent heat of melting. This leads to the expression

$$\tau_b = \frac{\eta u_b}{\pi} \int_0^\infty \frac{\hat{B}(k) k_*^2 k^3}{k_*^2 + k^2} \, \mathrm{d}k, \qquad k_* = \frac{\rho L}{4 C k_b \eta}, \tag{3.79}$$

where $\hat{B}(k)$ is again the power spectrum of the bed roughness, and k_* should be interpreted as a controlling wavenumber, which can be identified with the reciprocal of the controlling obstacle size a (for $n = 1$). This is again the same as (3.70), with $m = 1$.

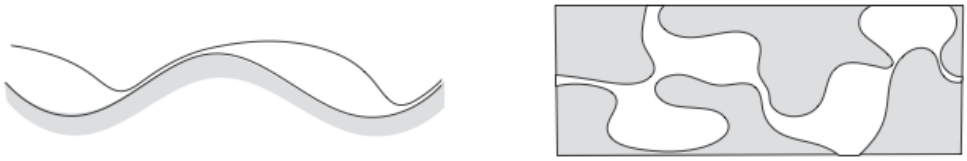

Figure 3.3: Cavitation behind bumps in bedrock viewed from the side and from above.

3.3.4 *Sliding on sediments

For a glacier lying on a layer of sediments, the sediments may deform under the action of the shear stress τ_b. If the sediment is treated as viscous, with effective viscosity η_T, and occupies a layer of depth d_T (below which is rigid bedrock), then the lubrication approximation suggests that the velocity profile through the sediment layer is linear, with no-slip at its base,

$$u_T = \frac{\tau_b}{\eta_T}(z - b + d_T), \qquad b - d_T \leq z \leq b. \tag{3.80}$$

(The till layer is assumed to be relatively thin, so that the shear stress may be taken as constant throughout it; otherwise there may be a quadratic Poiseuille-like component to this profile too, driven by the weight of the sediments). If there is no slip between the ice and the top of the sediments, so $u_b = u_T|_{z=b}$, this gives rise to an effective sliding law

$$\tau_b = \frac{\eta_T}{d_T} u_b. \tag{3.81}$$

The constitutive law for deforming sediments is not well constrained by measurements. There is some suggestion that a power law may be appropriate (as for ice), but other suggestions that a perfectly plastic description is better (this corresponds to taking the power law exponent to infinity), in which case the concept of the effective viscosity η_T is less useful.

In either case, a crucial control appears to be played by the *effective pressure* in the sediments. This is the difference between the overburden pressure (roughly the cryostatic pressure $p = \rho g H$) and the pore water pressure p_w. The effective pressure is commonly denoted $N = p - p_w$, and the till viscosity is thought to be an increasing function of N. This suggests a modified sliding law of the form

$$\tau_b = f(u_b, N), \tag{3.82}$$

with $\partial\tau_b/\partial u_b > 0$ and $\partial\tau_b/\partial N > 0$. The question then is what controls the effective pressure, and this is a subject discussed below in the context of subglacial drainage.

3.3.5 Cavitation

Even for hard-bedded glaciers the water pressure, or more precisely the effective pressure, is thought to exert a strong control on sliding, which is not captured by the Weertman law (3.70). The reason for this is the formation of water-filled 'cavities' at the bed.

As ice slides over small obstacles in the bed, we noted earlier that this results in elevated pressure on the upstream faces and reduced pressure on the downstream faces. If the pressure on the downstream face is low enough it causes the ice to separate from the rock, forming a water-filled cavity in the lee side of the obstacle. The size of such cavities depends on the

effective pressure N. If the water pressure in the cavities is very low (meaning N is large) then the cavities will be small, or perhaps non-existent. If the water pressure is as large as the average overburden pressure (so $N = 0$) the cavities can enlarge to cover almost the entire bed. Consideration of the viscous flow of the ice over the cavities suggests that the controlling quantity is actually u_b/N^n; cavity size increases with this ratio.

Cavities reduce the contact area between ice and bed, and therefore decrease the resistance to flow for a given sliding speed. Thus, as for sliding over sediments, we expect a sliding law of the form in (3.82). Two such laws that are in common usage are a generalised Weertman law,

$$\tau_b = C u_b^{1/m} N^{1/p}, \tag{3.83}$$

and a Coulomb-limited law,

$$\tau_b = \mu N \left(\frac{u_b}{u_b + \Lambda N^n} \right)^{1/n}, \tag{3.84}$$

which has the property that τ_b can't exceed a maximum value μN regardless of how fast the ice slides. Such behaviour, with $\tau_b = \mu N$ is the same as Coulomb friction, a common model of sliding friction in many other contexts.

These modified sliding laws are only able to provide the necessary link between basal velocity and shear stress if the effective pressure, or equivalently the water pressure, is known. This emphasises the importance of subglacial water, to which we now turn.

3.4 Subglacial drainage

The bottom of a glacier is usually a wet place. Geothermal heating, and frictional heating due to sliding, cause the temperature over most of the bed to be at the melting point, with melting rates from the bottom of the ice on the order of mm to cm per year. In addition, large quantities of water from the ice surface reach the bed through crevasses and moulins (roughly cylindrical shafts). The ice surface often melts at rates of several m per year, and this melting is concentrated in a short period during the summer, so the volumes of water reaching the bed can be large.

Some of the subglacial water may flow into cracks in the underlying rock or into the pore space of subglacial sediments, but most of it must be evacuated by flowing along the ice-bed interface and emanating from the glacier terminus. It usually appears at the terminus as a stream flowing out of a tunnel incised into the ice, and it is thought that most of the drainage beneath the glacier occurs in a network of such tunnels analogous to a normal river network.

The theory for these subglacial tunnels - often called channels - was developed by Röthlisberger, after whom they are sometimes named. The channels are thought to open and close each year, since viscous deformation of the ice causes them to creep closed during the winter. In summer, heat generated by dissipation in the turbulent water flow causes them to enlarge again. This melting of the ice around the channel walls is analogous to the erosion that forms river channels; the interesting difference for the subglacial channels is that they creep closed whenever the discharge decreases and the melting is therefore reduced. River channels to not generally fill in so quickly when the discharge is low.

If the subglacial channels are equivalent to rivers, forming an artery-like drainage network, there must also be some equivalent of the distributed overland or groundwater flow that enables water to get into the channels. Sub-glacially this distributed flow is believed to occur by

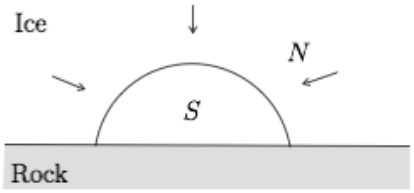

Figure 3.4: A subglacial channel.

seepage of water between the cavities that form behind bed bumps (as described in the previous section). There is evidence, both from beneath current glacier beds and from deglaciated bedrock, of the water flowing between these cavities, which act in effect as 'pores' of a macroscopic porous medium. The flow through the cavities can be modelled using a turbulent-flow generalisation of Darcy's law that describes flow in a porous medium.

We discuss the dynamics of channels and cavities in turn. An important concept in doing so is the hydraulic potential ϕ, which is given by

$$\phi = p_w + \rho_w g b. \tag{3.85}$$

Here p_w is the water pressure, ρ_w is the water density, g is the gravitational acceleration, and $z = b(x)$ is the bed elevation. The gradient of the potential provides the driving force for water movement (if the potential is constant, the pressure is hydrostatic so there is no movement).

Notice that in a river, where p_w is approximately equal to the constant atmospheric pressure, the gradient of ϕ is simply proportional to gravity times bed slope, which is the driving force used for modelling rivers. If the bed is flat, the potential gradient is the same as the pressure gradient and this corresponds to pressure-driven flow, along a pipe for example.

It is convenient to write the potential in terms of the effective pressure $N = p - p_w$, where $p = \rho g H$ is the hydrostatic ice pressure at the bed. Then,

$$-\frac{\partial \phi}{\partial x} = -\rho_w g \frac{\partial b}{\partial x} - \rho g \frac{\partial H}{\partial x} + \frac{\partial N}{\partial x}. \tag{3.86}$$

In some cases, particularly for mountain glaciers, the gradient of ϕ is dominated by the bed elevation and we can approximate it by

$$-\frac{\partial \phi}{\partial x} \approx \rho_w g \sin\theta, \tag{3.87}$$

where θ is the bed slope (cf. the driving gravitational force for river flow).

3.4.1 Subglacial channels

A model for the subglacial channels can be derived in a similar way to that for a river, based on the ingredients of mass conservation and force balance. In addition, since the size of the channel changes quite quickly, we need an equation for the evolution of its cross-section (equivalent to the Exner equation for a river).

We assume that the tunnel has a semi-circular cross-section, with area $S(x,t)$ and discharge $Q(x,t)$. Mass conservation is expressed as

$$\frac{\partial S}{\partial t} + \frac{\partial Q}{\partial x} = \frac{M}{\rho_w}, \tag{3.88}$$

where the source term on the right is due to the melting rate M of the ice from the tunnel walls It is also possible to include a source term due to seepage from the surrounding bed and due to water input from the surface through a moulin or crevasse, but we include the latter here as an upstream boundary condition instead.

Force balance is expressed as

$$\tau \ell = -S\frac{\partial \phi}{\partial x}, \tag{3.89}$$

where $\tau = f\rho_w U^2$ is the wall stress (different from the viscous shear stress in the ice, though the notation is the same), $\ell = S^{1/2}2^{1/2}(2+\pi)/\pi^{1/2}$ is the wetted perimeter, and $U = Q/S$ is the average water speed. This rearranges to give

$$FQ^2 = S^{5/2}\left(-\frac{\partial \phi}{\partial x}\right), \tag{3.90}$$

where $F = 2^{1/2}/(2+\pi)f\rho_w/\pi^{1/2}$.

The evolution equation for the cross-sectional area is written

$$\frac{\partial S}{\partial t} = \frac{M}{\rho} - \frac{2A}{n^n}SN^n, \tag{3.91}$$

where M is the wall melting rate, ρ is the ice density, N is the effective pressure and A and n are the coefficients in Glen's flow law, which describes the creep of the ice walls inwards. Finally, the melting rate is determined by an energy balance between the heat generated by turbulent dissipation in the water, given by $Q(-\partial\phi/\partial x)$, and the latent heat required to melt the walls, LM,

$$M = \frac{Q}{L}\left(-\frac{\partial \phi}{\partial x}\right). \tag{3.92}$$

Combining (3.88), (3.90), (3.91) and (3.92) provides a model for the evolution of the tunnel cross section and the effective pressure. It is forced by the input to the channel, which we take to be given as a boundary condition at the upstream end.

The equations can be simplified if we approximate the potential gradient as in (3.87). In this case, taking the steady-state version of (3.91), the equations can be re-arranged to find

$$N = \frac{n(\rho_w g \sin\theta)^{7/5n}}{\left(2A\rho L F^{2/5}\right)^{1/n}}Q^{1/5n}. \tag{3.93}$$

This implies an increasing relationship between discharge and effective pressure, so suggests that the water pressure will be lower for larger discharge ($p_w = p - N$). This is the opposite of our usual experience, when forcing more water through a pipe, for example, requires a larger water pressure. The reason is that this channel selects its own size; larger discharge results in a larger channel and less resistance as a consequence.

The increasing relationship between Q and N means that if two neighbouring channels are hydraulically connected (by seepage through sediments or cavities for example), water will

tend to move from the smaller one (which has a higher water pressure) to the larger one. This 'capturing' property of the channels means that at least locally the water focusses into one main channel; on a larger scale it leads to an arterial-like channel network, similar to a normal river network.

Note that the dependence of effective pressure on Q is rather weak, since $n \approx 3$, and a 1/15th power-law is almost indistinguishable from a constant unless Q changes over many orders of magnitude.

The relationship in (3.93) also allows us to estimate the size of the pressure gradient in (3.86) and check whether it was consistent to ignore that term. We find that this is a reasonable approximation except near the glacier terminus, where a boundary layer is necessary in order to satisfy the condition that the water pressure must equal atmospheric pressure there.

3.4.2 *Linked cavities

Flow between cavities can be described using a law of the form

$$Q \propto -K(h)\frac{\partial \phi}{\partial x}, \tag{3.94}$$

where Q is the discharge, and $K(h)$ is the hydraulic conductivity, which depends on the average depth of the water-filled cavities across the bed, h. This is very similar to Darcy's law, with the conductivity taking the place of the permeability.

The depth of the water-filled cavities depends on the roughness of the bed and, as discussed in the previous section, on the effective pressure and also the sliding speed. Thus we may take

$$h = h(u_b/N^n), \tag{3.95}$$

an increasing function of the ratio u_b/N^n. Since $K(h)$ is also increasing, this suggests that, for given potential gradient $-\partial\phi/\partial x \approx \rho_w g \sin\theta$, the discharge through the linked cavities decreases with N, *i.e.*

$$\frac{\partial Q}{\partial N} < 0. \tag{3.96}$$

This is different from the behaviour in the Röthlisberger channels, and helps explain why the water flow through cavities does not focus into a channel network.

This behaviour also implies that if all drainage occurs through the cavities and the water discharge increases (which it must do during summer to evacuate all the meltwater coming from the ice surface), the effective pressure must decrease. Returning to the sliding law of the previous section (3.82), this suggests that the sliding speed would increase when there is more water flowing (since the shear stress τ_b is determined by the ice depth so can't change quickly).

However, with larger discharge through the cavities it is possible for some of the larger ones to grow into Röthlisberger channels, and thus change the drainage system into a channel network through which the majority of the water flows. The discharge then becomes an increasing function of effective pressure (3.93), and so the sliding law indicates that the sliding speed decreases with more water.

This discussion helps to explain the confusing observation that some glaciers are seen to speed up during the summer whereas some are found to slow down. It makes predictions about how glacier speed will change in response to future climate particularly challenging.

3.5 Glacier surging

Glacier *surges* are sudden dramatic increases in the speed of a glacier that occur with an approximately regular period. The speed-up can be 100 fold (to speeds of around 10 km y^{-1}), and lasts for several months. During this period the glacier advances and thins. It is followed by a quiescent period, in which the glacier moves at a more usual glacial pace, and which lasts for several years or more. We attempt to understand this phenomena as a form of relaxation oscillation.

The most well-documented example of a surging glacier is Variegated glacier in Alaska, where a surge during 1982 and 1983 was studied with a large field campaign. There are, however, many hundreds of surging glaciers around the world. It is currently not known why some glaciers undergo this surging behaviour while others do not.

3.5.1 Drainage mechanism

A leading explanation for the surge behaviour is that it corresponds to a sudden change in the structure of the subglacial drainage system. The idea is that the surge corresponds to a state in which channel drainage is unstable and the water is forced to flow through an inefficient system of linked cavities. The cavity system results in smaller values of effective pressure which, according to the sliding law (3.82) result in faster sliding speeds. When a channel system dominates the drainage, the effective pressure is larger and the sliding speeds more subdued.

The reason why a channel-dominated drainage system might become unstable is a little mysterious, but is related to the size of the cavities. If the cavities become sufficiently large, the channels will shut down and all the water flows through the cavities. The critical parameter is therefore u_b/N^n, which controls cavity size. Below a certain value of this parameter, Λ_c say, channels are stable, and above it they are not.

We denote the effective pressure in a channel system and a cavity system by N_R and N_K respectively, and suppose that these are constants (they depend on the water discharge, but only weakly as noted earlier). The generalised Weertman sliding law (3.83) then gives the corresponding sliding velocities as

$$u_b = C^{-m}\tau_b^m N_R^{-m/p}, \qquad u_b < \Lambda_c N_R^n, \tag{3.97}$$

$$u_b = C^{-m}\tau_b^m N_K^{-m/p}, \qquad u_b > \Lambda_c N_K^n, \tag{3.98}$$

where the basal shear stress is $\tau_b \approx -\rho g H \sin\theta$. Note that since $N_R > N_K$, there is a range of sliding velocities over which both of these options are possible, and since u_b is controlled in each case by the basal shear stress this corresponds to a range of ice depths. The relationship between sliding speed and ice depth is therefore multivalued. Converting into a relationship between ice flux q and depth H (we ignore internal shearing of the ice, since the surge is associated with sliding), this gives

$$q = (\rho g \sin\theta/C)^m N_R^{-m/p} H^{m+1}, \qquad H < H_+, \tag{3.99}$$

$$q = (\rho g \sin\theta/C)^m N_K^{-m/p} H^{m+1}, \qquad H > H_-, \tag{3.100}$$

where $H_\pm = (C/\rho g \sin\theta)\Lambda_c^{1/m} N_{R/K}^{n/m+1/p}$.

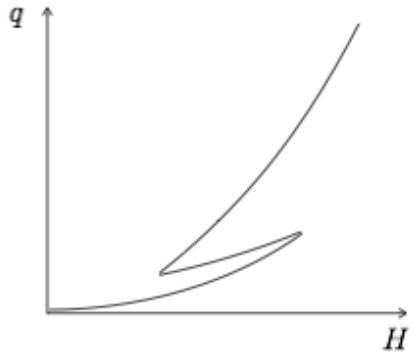

Figure 3.5: Multivalued relationship between ice thickness and flux.

The lower branch corresponds to the channel drainage system with slower sliding speed, and the upper branch corresponds to the cavity drainage system with faster sliding speed. Such a multivalued relationship can then be combined with the mass conservation equation,

$$\frac{\partial H}{\partial t} + \frac{\partial q}{\partial x} = a, \tag{3.101}$$

to explain the occurrence of surge cycles as follows.

The growing glacier occupies the lower branch of the ice flux/depth relationship, and gets thicker over time, growing towards a steady state that would require the ice to be thicker than H_+. Before it reaches the steady state, it therefore reaches the end of the lower branch; the channel drainage system shuts down and the glacier is forced onto the upper fast-moving branch. Only a small section of the glacier will have exceeded H_+ initially, but the theory goes that once some part of the ice has accelerated it forces the rest of the glacier with $H > H_-$ to move onto the upper branch too (this is due to the longitudinal stress that have been neglected in our lubrication theory, but which prevent there from being large downstream gradients in velocity). This corresponds to the initiation of the surge, which then causes the glacier to lengthen and thin (the steady state to which the glacier is now evolving has thickness $H < H_-$ since the same steady-state ice flux now requires thinner ice). Once the ice has thinned sufficiently it falls off the upper surging branch and returns to the lower branch. The quiescent period of slow thickening then begins again. The surge period is dominated by the slow growth from H_- to H_+, since the thinning during the surge occurs more rapidly.

3.5.2 *Thermal mechanism

A similar explanation of surges in terms of a multivalued ice flux-depth relationship is related to the thermal state of the glacier. The basic mechanisms of having two overlapping 'branches' of the relationship is the same, but in this case the slow branch corresponds to the glacier having a frozen bed and therefore little or no sliding, whereas the fast branch corresponds to the glacier having a temperate bed with rapid sliding. The cold branch operates at ice depths below a critical thickness H_+, beyond which the insulating effect of the ice allows its bed to be warmed to the melting point by geothermal heating. The increased frictional heating due to sliding when the bed is at the melting point means that the warm sliding state can operate

down to lower thicknesses $H > H_-$, so that there is again a range of depths for which both states are possible.

As a simple model to illustrate this we assume a conduction-dominated temperature profile (this is not usually a good model, since advection is also important, but it illustrates the point). In this case the steady-state temperature profile is governed by

$$0 = k\frac{\partial^2 T}{\partial z^2}, \qquad b < z < s, \tag{3.102}$$

with boundary conditions

$$T \le 0, \quad -k\frac{\partial T}{\partial z} = G \qquad \text{or} \qquad T = 0, \quad -k\frac{\partial T}{\partial z} \ge G + \tau_b u_b \qquad \text{at} \quad z = b, \tag{3.103}$$

and

$$T = T_s \quad \text{at} \quad z = s, \tag{3.104}$$

where G is the geothermal heat flux and $T_s < 0$ is the surface temperature.

In the cold-bedded case, $T = T_s + (G/k)(s - z)$, $u_b = 0$, and this applies while $H \le H_+ = kT_s/G$. In the warm-bedded case, $T = T_s(1 - (s - z)/H)$, $u_b \ge 0$ (related to τ_b by the sliding law), and this applies while $H \ge H_-$ where H_- satisfies $kT_s/H = G + \tau_b u_b$ (for example $kT_s/H_+ = G + C(\rho g \sin\theta)^m H_+^m$, using the Weertman sliding law (3.70) and $\tau_b = \rho g H \sin\theta$).

This thermal mechanism has been used on a larger scale to explain huge surges of the Laurentide ice sheet originating in Hudson bay during the last glacial period. These surges supposedly discharged vast quantities of ice bergs to the North Atlantic, which deposited frozen-on debris as they melted. The debris is recorded in layers of sediments taken from the ocean floor, and the deposition events are referred to as Heinrich events.

3.6 Ice sheets

The canonical model for an ice sheet is very similar to that for a glacier, but without a particular direction of bed slope. We consider an isothermal two-dimensional ice sheet, with net accumulation $a(x,t)$, bed elevation $z = b(x)$ and surface elevation $z = s(x,t)$, where x and z are now the horizontal and vertical coordinates. The expressions for mass conservation (3.6) and flux (3.15) therefore hold, together with the results for ice pressure, shear stress, and velocity profile,

$$p = \rho g(s - z), \qquad \tau = -\rho g(s - z)\frac{\partial s}{\partial x}, \tag{3.105}$$

$$u = u_b - \frac{2A(\rho g)^n}{n+1}\left|\frac{\partial s}{\partial x}\right|^{n-1}\frac{\partial s}{\partial x}\left(H^{n+1} - (s-z)^{n+1}\right), \tag{3.106}$$

$$q = u_b H - \frac{2A(\rho g)^n}{n+2}\left|\frac{\partial s}{\partial x}\right|^{n-1}\frac{\partial s}{\partial x}H^{n+2}, \tag{3.107}$$

$$\frac{\partial H}{\partial t} + \frac{\partial q}{\partial x} = a. \tag{3.108}$$

After non-dimensionalising, assuming no basal sliding and a flat bed $b = 0$ for simplicity, we have

$$\frac{\partial H}{\partial t} = \frac{\partial}{\partial x}\left[H^{n+2}\left|\frac{\partial H}{\partial x}\right|^{n-1}\frac{\partial H}{\partial x}\right] + a. \tag{3.109}$$

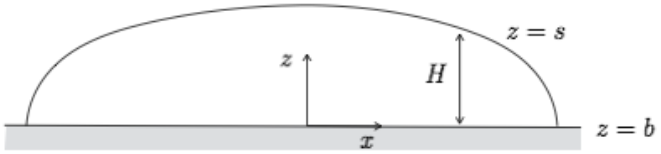

Figure 3.6: An ice sheet on a flat bed.

The generalisation to two horizontal dimensions, when $H = H(x, y, t)$, is

$$\frac{\partial H}{\partial t} = \nabla \cdot \left[H^{n+2} \left| \nabla H \right|^{n-1} \nabla H \right] + a, \tag{3.110}$$

where $\nabla = (\partial x, \partial y)$ is the two-dimensional gradient. Generalisations that allow sliding at the ice-sheet bed are straightforward to derive in the same way as for glaciers.

3.6.1 Steady states

Returning to one horizontal dimension, as for a glacier, a steady-state ice sheet terminating on land has boundaries x_{m-} and x_{m+} such that

$$\int_{x_{m-}}^{x_{m+}} a(x') \, \mathrm{d}x' = 0. \tag{3.111}$$

If we assume symmetry at $x = 0$, so $q = 0$ there, then the right-hand margin x_m is such that

$$\int_{0}^{x_{m}} a(x') \, \mathrm{d}x' = 0, \tag{3.112}$$

and the ice thickness is given by

$$H^{n+2} \left(-\frac{\partial H}{\partial x} \right)^n = \int_0^x a(x') \, \mathrm{d}x'. \tag{3.113}$$

Assuming $H = 0$ at $x = x_m$, this can be integrated to give

$$H_0(x) = \left[\int_x^{x_m} \frac{2(n+1)}{n} \left(\int_0^{x''} a(x') \, \mathrm{d}x' \right)^{1/n} \mathrm{d}x'' \right]^{n/2(n+1)}. \tag{3.114}$$

The situation is different if the ice sheet terminates in the ocean, because in this case neither the ice thickness nor the flux need be zero there, so the condition that the integrated accumulation should be zero no longer holds. Instead, if q_m is the ice flux at the margin x_m, we have (in a steady state),

$$\int_0^{x_m} a(x') \, \mathrm{d}x' = q_m. \tag{3.115}$$

This ice flux might break off immediately as icebergs, or it might flow into a floating ice shelf that is attached to the end of the ice sheet. In this case, x_m is referred to as the *grounding line*, since it is where the ice shelf grounds on the sea floor.

A detailed theory of the flow across the grounding line (see below) suggests that it may be reasonable to impose $q_m = Q_m(x_m)$ as a known function of space, and to impose $H(x_m) = H_m \approx 0$. (The reason for this is that the stress balance where the ice becomes afloat forces the ice thickness and flux to take certain values that depend on the depth of the water there, but the ice thickness is relatively small and can be approximated as zero). In this case the net mass balance statement (3.115) still determines the position of the margin, as for the land-terminating ice-sheet. If $H_m = 0$, then (3.114) also determines the ice thickness.

3.6.2 *Plastic ice

A useful simplification of the model occurs in the limit $n \to \infty$, which corresponds to a perfect plastic. That is, the constitutive law becomes

$$\dot{\varepsilon}_{ij} = 0, \quad \tau \leq \tau_c \qquad \text{or} \qquad \dot{\varepsilon}_{ij} \propto \tau_{ij}, \quad \tau = \tau_c. \tag{3.116}$$

This states that the ice is completely rigid and does not deform if the stress invariant τ is below the *yield stress* τ_c, but that if the yield stress is reached it can deform readily to prevent the stress exceeding this value. To those familiar with Newtonian fluids, this may seem strange, and it presents problems for some numerical methods because it can in principle allow very large strain rates. In practice it is sometimes regularised using a power-law with large n.

Within the shallow ice approximation, the stress invariant is the same as the shear stress

$$\tau = -\rho g H \nabla s, \tag{3.117}$$

so the plastic rheology demands that either the ice is stationary, or

$$\frac{\tau_c}{\rho g} = -H|\nabla s|. \tag{3.118}$$

In two-dimensions, and with a flat bed, this is

$$\frac{\tau_c}{\rho g} = -H\frac{\partial H}{\partial x}, \tag{3.119}$$

with solution

$$H = \left(\frac{2\tau_c}{\rho g}\right)^{1/2} (x_m - x)^{1/2}, \tag{3.120}$$

where x_m is the position of the margin, at which we have assumed $H = 0$.

3.6.3 Marine ice sheets

Large parts of the Antarctic ice sheet have the bed below sea level. The ice sheet is surrounded by a floating ice shelf, which melts from underneath, and breaks off as ice bergs from its edge. The boundary between the grounded ice sheet from the floating ice shelf is called the grounding line. The ice flux across the grounding line is particularly important for determining sea-level changes, since once the ice is afloat it has very little impact on sea level (it occupies the same volume of the ocean as will the water once it has melted).

We consider a simplified model of a marine ice sheet that treats the ice as a Newtonian fluid, and assume that its motion is dominated by sliding at the base according to the linear

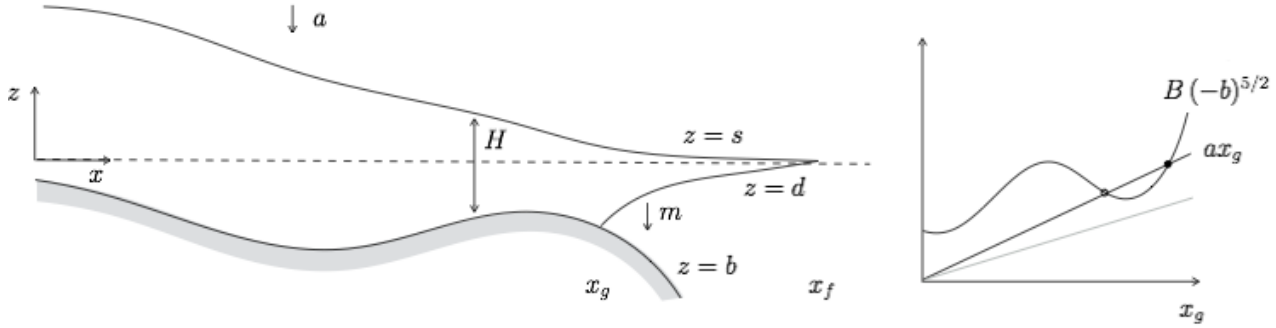

Figure 3.7: A marine ice sheet, with grounded ice and floating ice shelf. The panel on the right shows possible steady state configurations according to (3.134).

Weertman sliding law $u_b = C\tau_b$. We assume a known bed topography $z = b(x)$, measured relative to sea level, with an ice divide located at $x = 0$. The ice thickness over the grounded ice evolves according to

$$\frac{\partial H}{\partial t} + \frac{\partial q}{\partial x} = a, \qquad q = uH = -C\rho g H^2 \frac{\partial s}{\partial x}, \tag{3.121}$$

with $q = 0$ at $x = 0$. The grounding line x_g occurs where the ice becomes afloat, so $\rho g H = -\rho_w g b$ there (i.e. the weight is balanced by the weight of the water according to Archemides' principle; ρ_w is the density of the ocean water). Therefore

$$H = -\frac{\rho_w}{\rho} b, \qquad \text{at} \quad x = x_g. \tag{3.122}$$

However, since x_g is a free boundary to be determined, we need one further condition there. This comes from ensuring a balance of the longitudinal forces with the ice in the ice shelf, which we consider next.

The ice shelf does not touch the bed, so we introduce the notation $z = d(x, t)$ to denote the elevation of its base. Since the ice is floating, this satisfies $\rho g H = -\rho_w g d$, and hence the surface elevation is related to the ice thickness by

$$s = d + H = \left(1 - \frac{\rho}{\rho_w}\right) H. \tag{3.123}$$

Unlike the grounded ice, horizontal stresses are small within the ice shelf, and we must include the extensional stresses (which were previously neglected) in the force balance. The relevant approximation of the horizontal momentum equation is

$$\frac{\partial}{\partial x}\left(4\eta H \frac{\partial u}{\partial x}\right) - \rho g H \frac{\partial s}{\partial x} = 0. \tag{3.124}$$

(This model is similar to those used for free viscous sheets and fibres, such as occur in a number of manufacturing processes). Combining (3.123) and (3.124), we have

$$\frac{\partial}{\partial x}\left[4\eta H \frac{\partial u}{\partial x} - \frac{1}{2}\rho g \left(1 - \frac{\rho}{\rho_w}\right) H^2\right] = 0, \tag{3.125}$$

and assuming that the ice thickness goes to zero at the downstream end of the ice shelf, this can be integrated to give

$$4\eta H\frac{\partial u}{\partial x}=\frac{1}{2}\rho g\left(1-\frac{\rho}{\rho_w}\right)H^2, \tag{3.126}$$

throughout the ice shelf. This is to be solved together with the mass conservation equation

$$\frac{\partial H}{\partial t}+\frac{\partial q}{\partial x}=a-m, \qquad q=uH, \tag{3.127}$$

where we have added the basal melting rate m as a mass sink. The end of ice shelf x_f occurs where the ice flux goes to zero, so

$$q=0, \qquad \text{at} \quad x=x_f. \tag{3.128}$$

Continuity of longitudinal stress requires that the ice-shelf stress balance (3.126) must apply at the grounding line, where the stretching rate $\frac{\partial u}{\partial x}$ can be evaluated from upstream. This requires that the stretching rate becomes large, which happens over a relatively small length scale on which the flux q may be assumed to be constant and on which the gradient of the bed slope may be ignored (we don't show this here). Therefore, recalling that $q=uh$,

$$\frac{\partial u}{\partial x}\approx-\frac{u}{H}\frac{\partial H}{\partial x}\approx-\frac{u}{H}\frac{\partial s}{\partial x}=-\frac{q^2}{C\rho g H^4}, \tag{3.129}$$

where the last equality follows from $(3.121)_2$. Inserting this expression into (3.126) and rearranging leads to

$$q=\left[\frac{C(\rho g)^2(1-\rho/\rho_w)}{8\eta}\right]^{1/2}H^{5/2} \qquad \text{at} \quad x=x_g, \tag{3.130}$$

or, combining with the flotation condition (3.122),

$$q=B\,(-b)^{5/2} \qquad \text{at} \quad x=x_g. \tag{3.131}$$

where $B=[C\rho_w^5 g^2(1-\rho/\rho_w)/8\eta\rho^3]^{1/2}$.

As an example, consider a steady state with uniform accumulation rate a and uniform melt rate $m>a$ beneath the ice shelf. The steady state mass balances require

$$q=ax \qquad 0<x<x_g, \tag{3.132}$$

$$q=ax_g-(m-a)(x-x_g), \qquad x_g<x<x_f, \tag{3.133}$$

with $x_f=mx_g/(m-a)$. The ice thickness can then be calculated by integrating $(3.121)_2$ backwards from the grounding line, where $H=-(\rho_w/\rho)b(x_g)$, and integrating (3.126) forward from the grounding line with $u=q/H$. The position of the grounding line itself is determined from the condition (3.131), which requires

$$ax_g=B(-b(x_g))^{5/2}. \tag{3.134}$$

Depending on the shape of the bedrock, there may be multiple possible steady state grounding line positions, and changing the accumulation rate can result in these states appearing or disappearing. This may explain some of the very rapid sea level rise that has occurred in the past, when large sections of previously floating ice become afloat as the grounding line retreats.

3.6.4 *Accumulation-elevation feedback

An interesting aspect of ice sheets is that their surface elevation is essentially self-determined, unlike a glacier where the surface elevation is largely set by the bed elevation. The ice in an ice sheet is usually much thicker, and the surface topography does not necessarily bear much resemblance to the bed topography. This means that the net accumulation a, which depends strongly on the air temperature at the surface, is not externally prescribed; it depends on the solution H.

In fact it does so in a way that generically suggests 'blow-up' behaviour, since we would expect a to be an increasing function of H, and the mass conservation equation becomes

$$\frac{\partial H}{\partial t} = \frac{\partial}{\partial x}\left[H^{n+2}\left|\frac{\partial H}{\partial x}\right|^{n-1}\frac{\partial H}{\partial x}\right] + a(H). \tag{3.135}$$

The equivalent linear problem would be the reaction diffusion equation,

$$\frac{\partial H}{\partial t} = \frac{\partial^2 H}{\partial x^2} + H. \tag{3.136}$$

Our nonlinear generalisation of this equation has the same general property that the 'reaction' term can cause blow-up ($H \to \infty$), perhaps limited by the diffusion term depending on the size of the domain. The ice sheet also has a free boundary, and the reaction term can therefore lead to an ice sheet that grows ever wider and thicker. In reality, it is limited either by flowing into the ocean or by spreading to low enough latitudes that the net accumulation becomes sufficiently negative to balance the increased accumulation at the surface.

A simple toy model that illustrates dependence of accumulation on surface elevation and latitude is to take $n = 1$ (Newtonian ice) and

$$a = \frac{1}{4}(H^4 - x). \tag{3.137}$$

Here x can be considered as distance from the pole, and we assume the ice grows symmetrically from $x = 0$ (though in one horizontal dimension still, for simplicity). The steady state then satisfies

$$0 = \frac{\partial}{\partial x}\left(H^3\frac{\partial H}{\partial x}\right) + \frac{1}{4}(H^4 - x), \tag{3.138}$$

with boundary conditions

$$H^3\frac{\partial H}{\partial x} = 0 \quad \text{at} \quad x = 0, \qquad H^3\frac{\partial H}{\partial x} = H = 0 \quad \text{at} \quad x = x_m. \tag{3.139}$$

These three conditions serve to determine the position of the margin x_m.

Letting $y = H^4$, the problem simplifies to

$$x = \frac{\partial^2 y}{\partial x^2} + y. \tag{3.140}$$

with

$$\frac{\partial y}{\partial x} = 0, \quad \text{at} \quad x = 0, \qquad \frac{\partial y}{\partial x} = y = 0 \quad \text{at} \quad x = x_m. \tag{3.141}$$

The solution is found to be

$$y = x - \sin x + \frac{1 - \cos x_m}{\sin x_m} \cos x, \tag{3.142}$$

where x_m satisfies

$$x_m \sin x_m = 1 - \cos x_m. \tag{3.143}$$

In fact there are two viable solutions here; ones has $x_m \approx 2.33$, and the other has $x_m = 0$. The latter solution corresponds to there being no ice at all. One of the features of the accumulation-elevation feedback is that there can be multiple steady states. It is believed that the current environment of the Greenland ice sheet probably gives rise to such multiple states. The ice sheet is relatively close to an equilibrium (though by no means in equilibrium; it is losing mass quite quickly), but if all the ice were somehow removed instantaneously it is unlikely it would grow back under present conditions. The climate of Antarctica on the other hand is sufficiently cold that were that ice sheet to be suddenly removed, at least a large part of it would grow back again.